Enhancement of hydrodeoxygenation catalytic performance through the addition of copper to molybdenum oxide-based catalysts

Débora G.B. Dionizio, Leticia Forrer, Gilles Berhault, Priscilla de Souza, Cristiane Henriques

Enhancement of Hydrodeoxygenation Catalytic Performance through the Addition of Copper to Molybdenum Oxide-Based Catalysts

Débora G. B. Dionizio[1,2]; Leticia Forrer[2]; Gilles Berhault[3]; Priscilla M. de Souza[2,4]; Cristiane A. Henriques[1*]

1-Universidade do Estado do Rio de Janeiro, Instituto de Química, Programa de Pós-Graduação em Engenharia Química (PPGEQ), Rua São Francisco Xavier, 524, PHLC, sl. 400; RJ, 20550-013, Brasil.

2-Universidade Federal do Rio de Janeiro, COPPE, Programa de Engenharia Química, RJ, 21941-972, Brasil.

3-Ircelyon, 2 Avenue Albert Einstein, Postal Code 69626, Villeurbanne, Lyon, France.

4- Univ. Lille, CNRS, ENSCL, Centrale Lille, Univ. Artois, UMR 8181 - UCCS - Unité de Catalyse et Chimie du Solide, F-59000, Lille, France.

* Corresponding author. Fax: + 55 21 3938 8344

E-mail address: cristihenriques@terra.com.br

Graphical abstract

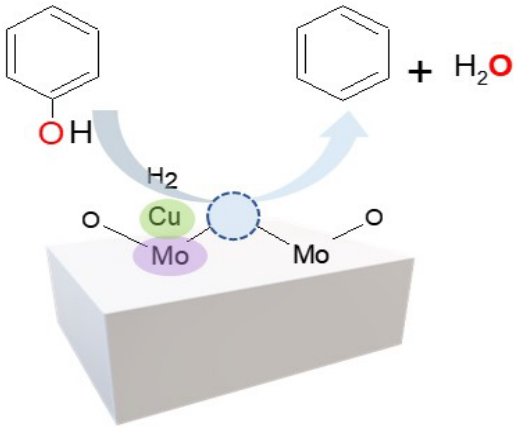

Highlights

- Bulk and supported molybdenum catalysts show high selectivity for benzene (~ 100 %).
- The carbon support promotes the reduction of molybdenum even under an N_2 atmosphere.
- Both carbon support and the addition of copper favor phenol conversion.
- CuMo/C is the most active and selective catalyst for HDO of phenol.
- A correlation between the HDO rate and the number of oxygen vacancies is observed.

Abstract

The role of copper promoter and carbon support on the activity, selectivity, and stability of molybdenum oxide was determined for bulk and carbon-supported molybdenum oxide catalysts in phenol hydrodeoxygenation (HDO). The catalytic performance was correlated to the physicochemical properties determined using ICP-AES, XRD, XPS, Raman, TPR, H_2O-TPD, and oxygen chemisorption. The results showed that at the studied reaction conditions (atmospheric pressure, 330 ºC, gas phase), the employment of activated carbon as support and the addition of copper improved phenol conversion from 1 (with MoO_3) to 28 % (with CuMo/C), maintaining high selectivity to benzene (around 100 %) while characterization studies evidence the formation of mainly $CuMoO_4$ species in bulk samples and metallic copper, Cu_2O, and MoO_2 on carbon-supported ones. The incorporation of copper in the molybdenum oxide catalysis promoted the reduction of molybdenum, the creation of oxygen vacancies, and the H• formation, all factors favoring the selective C-O bond cleavage. Stability tests of the most active catalysts, Mo/C_H_2 and CuMo_H_2, showed that deactivation happened, but the direct deoxygenation route remained preferential throughout the reaction time with high selectivity to benzene (up to 98 %). Deactivation was related to the lower concentration of available active sites (oxygen vacancies).

Keywords: Phenol; hydrodeoxygenation; molybdenum; copper, oxygen vacancies.

1. Introduction

Lignocellulosic biomass has recently arisen as an eco-friendly source to produce energy, biofuels, and chemicals of industrial interest [1–3]. This raw material can be processed using rapid pyrolysis, generating bio-oil as the main product. However, this bio-oil presents complex chemical composition and a high concentration of oxygenated compounds, around 35-40 wt. %, regardless of the origin of biomass and reaction conditions. These characteristics give this pyrolyzed product undesirable properties for its direct application as biofuels, such as high acidity and viscosity, low calorific value, thermal and chemical instability, and immiscibility with hydrocarbons [4,5].

To improve the biofuels characteristics, oxygen removal can be achieved by different physical methods, such as solvent addition, emulsification, filtration, vacuum distillation, extraction, and high-pressure homogenization, or chemical methods, for example, esterification, catalytic cracking, fast catalytic pyrolysis, catalysis in supercritical fluids, and hydrodeoxygenation (HDO) [4]. The catalytic hydrodeoxygenation represents a promising route for converting bio-oil into products with high added value. However, one limitation of this approach results from the high level of hydrogen consumption necessary for performing HDO. Therefore, one of the most important challenges related to this process is achieving a high rate of oxygen removal while maintaining a low rate of hydrogen consumption [5–7].

Due to the complexity of bio-oil, model molecules representative of compounds derived from the pyrolysis of biomass, such as phenol, anisole, cresol, and guaiacol, representing about 25 % of the oxygenated compounds derived from lignin fractions, are often used to elucidate and understand of the HDO kinetics and reaction mechanism [8–14].

Different catalysts have been tested to optimize this reaction. Transition metal sulfide catalysts, traditionally used in the hydrotreatment process (CoMoS and NiMoS), show good

conversion. However, these systems require high H_2 pressure conditions and continuous sulfur addition to preserve the active sites. Consequently, sulfur contamination of the desired products is often encountered, requiring further purification treatment to remove the sulfur contaminant [5,9]. Studies have shown that noble metals have higher activity in bio-oil HDO than nickel and molybdenum sulfide catalysts under the same conditions. However, the high cost and difficulty of recovery limit their industrial application [15–17]. The use of phosphides, carbides, and nitrides as catalysts for oxygen removal reactions has also attracted attention because these materials present activity similar to sulfides, besides having catalytic properties similar to those of a noble metal, such as good thermal and chemical stability. Nevertheless, these catalysts also present some disadvantages like complex methods of preparation and/or oxidation deactivation issues caused by the presence of water produced in the HDO process [18,19].

Therefore, the great challenge of the HDO process is to achieve a high degree of oxygen removal with low hydrogen consumption while adjusting catalyst activity and stability [6,10]. Molybdenum-based catalysts are selective in breaking C-O bonds under low H_2 pressure (which prevents saturation of the aromatic rings of lignin-derived compounds) while presenting a high water tolerance and a good resistance to coke formation [10–13,20–22]. Table S1 summarizes the studies on HDO of different model molecules derived from lignin using Mo-based catalysts and the experimental conditions used. In addition, different supports (transition metal oxides, carbon or mesoporous silica materials, etc.) and metal promoters (Co, Ni, Cu) on Mo-based catalysts have been investigated [15,16,23].

The Román-Leshkov group has studied the HDO performance of molybdenum oxide catalysts, both as bulk or supported MoO_3, in the gas phase, atmospheric pressure, and low temperature (320 – 400 ºC) HDO conditions [10–12,22]. Molybdenum oxide exhibits redox properties and can be used in short-chain oxygenated HDO processes. In addition,

molybdenum has low electron density and high electrophilicity, promoting the preferential adsorption of oxygen from the C=O bond, thus facilitating the hydrogenolysis step [24]. In its bulk form, this oxide has proved to be quite effective in the hydrodeoxygenation of several molecules derived from biomass, producing mainly olefinic and aromatic hydrocarbons [10]. On the other hand, MoO_x catalysts supported on SiO_2, γAl_2O_3, TiO_2, ZrO_2, and CeO_2 were very selective for the cleavage of the C-O bond of m-cresol without aromatic ring hydrogenation [12]. As stated by these authors, the HDO reaction follows the reverse Mars-van Krevelen reaction route, with the elimination of the oxygen atom from the reactant through its adsorption on a surface vacancy and the concomitant regeneration of the vacancy by reaction with H_2, producing water. Moreover, consistent with this description, the deactivation would be related to the reduction of MoO_3 to MoO_2.

Contrary to this latter assumption, controversial studies can also be found in which MoO_2/C catalysts were shown to be active in hydrodeoxygenation and selective to the cleavage of the C-O bond without causing the saturation of C=C bonds leading to the reduction of hydrogen consumption during the reaction. Additionally, MoO_2 was more resistant to carbon monoxide formation and water poisoning [13,20,21]. According to Ansaloni et al. (2017), oxygen vacancies, also called coordinatively unsaturated sites (CUS), generated by the surface reduction of some Mo (IV) species would be the active and selective sites responsible for the quite good performance of MoO_2/C in HDO of guaiacol at 350 °C and 4 MPa of H_2 [21]. However, these vacancies are not expected to be formed at low temperatures due to the low reducibility of MoO_2. Furthermore, the surface modification induced by the CUS formation influences not only the activity of the catalyst but also the selectivity of the products formed.

Following the same reasoning that oxygen vacancies would also be responsible for the activity of MoO_3, Kasiraju & Grabow (2018), based on Density Functional Theory (DFT)

calculations, evaluated the influence of different promoters (Fe, Co, Ni, Cu, Zn) added to MoO_3 on its catalytic activity for the HDO of furan [25]. In line with computational calculations, adding these promoters favors the thermodynamic tendency to form oxygen defects, even without a hydrogen atmosphere. At the same time, these surface modifications also decrease the activation barrier for splitting H_2, suggesting an enhanced rate of formation of oxygen vacancies. Among the promoters studied, the deposition of copper on the surface of MoO_3 was found to be more effective, favoring a more significant decrease in the activation energy barrier for vacancies formation. Moreover, the same authors state that the studied promoters also have a beneficial effect by avoiding the over-reduction of MoO_3 to MoO_2 while maintaining the ability to form vacancy sites. Indeed, Mo atoms at the top layer of the promoted MoO_3 (010) surface would be replaced by promoter atoms (Fe, Co, Ni, Cu, Zn) with a preferential substitution of Mo atoms at the O edge. This replacement would lead to a lower oxygen coverage on the promoted MoO_3 surface while increasing the number of metal atoms accessible on the surface, facilitating the H_2 activation. In contrast, the reduction of unpromoted MoO_3 would lead to an inactive HDO phase attributed to the distorted-rutile crystal structure of MoO_2. Although Cu has been indicated as the most effective promoter for forming oxygen vacancies in MoO_3, only two papers in the literature evaluated this catalyst in the liquid phase HDO reaction and none in the gas phase (Table S1, lines 26 and 27).

In this context, in the present study, bulk molybdenum oxides and molybdenum oxides supported on activated carbon were studied as catalysts for the HDO of phenol (in the gas phase at 330 ºC and atmospheric pressure). The introduction of a small amount of copper (Cu/Mo molar ratio = 0.1) in bulk and supported molybdenum catalysts was also evaluated to investigate its influence on the active sites and activity and selectivity of the reaction. Inductively Coupled Plasma – Atomic Emission Spectroscopy (ICP-AES), X-ray

diffraction (XRD), X-ray photoelectron spectroscopy (XPS), Raman spectroscopy, Temperature-Programmed Reduction (TPR), H_2O-Temperature Programmed Desorption (TPD), and oxygen chemisorption were also herein employed to evaluate the nature of the molybdenum and copper phases and to identify the formation of oxygen vacancies. Correlation between structure and activity has been established to provide new insights into the catalytic performance of Mo oxide-based catalysts for HDO applications.

2. Experimental

2.1 Catalyst Synthesis

Bulk MoO_3 (≥ 99.5%) was purchased from Sigma-Aldrich and used as received. The CuMo catalyst was prepared by incipient wetness impregnation of bulk MoO_3 (5 g) using an aqueous solution of $Cu(NO_3)_2.3H_2O$ (Sigma-Aldrich, ≥ 99%) to obtain the desired Cu/Mo molar ratio of 0.1. After impregnation, the sample was dried at 110 ºC overnight and calcined under airflow (60 mL min^{-1}) at 500 ºC (10 ºC min^{-1}) for 3 h.

The activated carbon was provided by Merck (K41944786) and used to prepare supported molybdenum oxide catalysts. Mo/C (13 wt. % Mo) was prepared by incipient wetness impregnation of the activated carbon (20 g), using an aqueous solution of $(NH_4)_6Mo_7O_{24}.4H_2O$ (Merck, ≥ 99,0%) (0.163 g mL^{-1}). For the bimetallic CuMo/C catalyst (Cu/Mo molar ratio = 0.1), the addition of copper was carried out by successive impregnation of dried Mo/C (10 g) using an aqueous solution of $Cu(NO_3)_2.3H_2O$ (1.03 g mL^{-1}). The Cu/C (13 wt. %) was prepared by adding dropwise the aqueous solution of $Cu(NO_3)_2.3H_2O$ (with the desired content of the copper) onto the activated carbon (10 g).

After the impregnation step, Mo/C, CuMo/C, and Cu/C catalysts were dried at 110 ºC overnight and then heated under N_2 (60 mL min^{-1}) (Air Products, 99.999%) at 10 ºC min^{-1} up to 500 ºC and kept at the final temperature for 3 h.

2.2. Catalyst Characterization

Molybdenum and copper loadings were determined by inductively coupled plasma optical emission spectrometry (ICP-OES) using an Activa-S spectrometer, HORIBA JOBIN YVON Scientific. Before the analysis, the bulk and carbon-supported samples were digested with H_2SO_4 and HNO_3 heated at 350°C – 400 °C.

The BET specific area of the samples was determined by nitrogen physisorption, at -196 ºC, in an ASAP 2020 equipment, Micromeritics. Each sample was previously treated under vacuum (0.1 mPa) at 300 °C for 3 h to ensure the elimination of water and other possible adsorbed contaminants.

X-ray diffraction patterns were collected on a Bruker D5005 instrument with nickel-filtered Cu Kα radiation (λ = 1.5418 Å) using the following parameters: 2θ = 10−80°; scan rate = 0.04°/step; and a scan time= 0.5 s/step. The diffraction patterns were normalized to the maximum peak intensity for each catalyst.

X-ray photoelectron spectroscopy (XPS) was performed on an Axis Ultra DLD (Kratos Analytical). Spectra were obtained using Al Kα radiation (1486.6 eV), with a fixed pass energy of 40 eV. Before moving to the XPS chamber, the samples were pressed onto an In foil connected to the sample. The binding energies were corrected at the C1s level of contaminant carbon at 284.6 eV with an uncertainty of 0.2 eV.

The decomposition of the Mo 3d and Cu 2p XPS spectra was performed considering Gaussian and Lorentzian mixed functions for the shape of the assembly curve line. After the background treatment, this assembly procedure was done using a Shirley baseline (CasaXPS software, version 2.0.71). The atomic percentage [i] of each element was obtained by measuring the corresponding total peak area $A_{i,}$ using appropriate sensitivity factors S_i.

$$[i] = \frac{\frac{A_i}{S_i}}{\sum_{i=1}^{n}(\frac{A_i}{S_i})}$$

Core level spectra of Mo 3d and Cu 2p were decomposed into three contributions corresponding to Mo IV, Mo V, and Mo VI species and two contributions associated with Cu I and Cu II species, respectively. The binding energy of copper species, Cu(0) and Cu (I), are too close, so the Auger parameter was determined to distinguish the copper species.

Raman spectroscopy was carried out on a HORIBA Jobin Yvon Labram HR spectrometer equipped with a Czerny-Turner monochromator and a charge-coupled device (CCD) detector cooled with liquid nitrogen. The excitation was provided by the 514 nm line of an Ar^+–Kr^+ ion laser with a maximum power fixed at 1.06 mW. The acquisition was carried out using a network of 300 lines.mm^{-1}. Before each series of data recordings, the calibration was performed with a silicon reference (characteristic vibrational mode at 521 cm^{-1}). The spectra were generally collected between 200 and 1200 cm^{-1} except for the carbon-supported catalysts for which the 150 - 3500 cm^{-1} wavenumbers range. The spectra of each catalyst were normalized to the maximum peak intensity to study the dispersion of Mo species on the surface of the support.

Temperature programmed reduction (TPR) was performed using a dynamic system connected to a mass spectrometer (Pfeiffer Vacuum, model TMU 071 P). The quartz U-tube was loaded with 0.1 g of catalyst in a typical procedure. Before the reduction, the catalyst was dried under a 50 ml min^{-1} flow of helium (Air Products, 99.999 %) to 200 ºC (10 °C min^{-1}) for 1 h. Heating was then ceased, and after reaching room temperature, the system was heated again to 1000 °C (heating rate of 10 °C min^{-1}) under a pure flow of H_2 (100 mL min^{-1}). During the reduction, the evolution of H_2O (m/z = 18), CO (m/z = 28), CO_2 (m/z = 44), and CH_4 (m/z = 15) were monitored using mass spectrometry.

Oxygen chemisorption was performed, according to the protocol proposed by Shetty and collaborators (2015), to determine the number of redox-active Mo sites and initial site time yields (STYs) [12]. The measurements of O_2 adsorption isotherms at 196 ºC were carried out using a Micromeritics 3Flex instrument. Prior to the analysis, the samples were treated in He flow (50 mL min^{-1}) at 120 ºC (5 ºC min^{-1}) for 30 min and then pre-reduced in a flow of H_2 (50 mL min^{-1}) for 2 h at 350 ºC (5 ºC min^{-1}). Previously to oxygen adsorption, the chemisorption cell was evacuated (67 Pa) for 2 h. After the first adsorption isotherm was acquired, weakly adsorbed O_2 was removed by degassing, and the adsorption isotherm was collected again. The irreversibly adsorbed O_2 was determined by extrapolating the difference between the first and second isotherms to zero pressure. The amount of redox-active Mo species (Redox-Mo) was obtained through equations 1 and 2.

$$Mols\ of\ Redox-Mo = 2 \times oxygen\ uptake\ (mol\ g^{-1}) \times catalyst\ mass\ (g)$$

(Equation 1)

$$Redox-Mo\ (\%) = \frac{2 \times oxygen\ uptake\ (mol\ g^{-1})}{Mo\ loading\ (mol\ g^{-1})} \times 100$$

(Equation 2)

H_2O-TPD was performed according to Gonzalez and coworkers (2019) using a multipurpose unit AutoChem 2920 Micromeritics coupled to a mass spectrometer Pfeiffer Vacuum OmniStar [26]. Initially, 0.2 g of catalyst was loaded in the reactor and dried at 130 ºC under He flow (30 mL min^{-1}) for 30 min. Then, the sample was treated with H_2 (50 mL min^{-1}) at 360 ºC (10 ºC min^{-1}) for 1 h and purged with He for 1 h at 360 ºC. Next, the H_2O adsorption was conducted at 40 ºC for 1 h. The H_2O vapor (75 kPa) was produced by passing He (50 mL min^{-1}) through a saturator containing deionized water kept at 40 ºC. Finally, the desorption was carried out employing a He flow (50 mL min^{-1}) from 40°C to 400 ºC (10 ºC

min^{-1}). The m/z = 2 (H_2) and m/z = 18 (H_2O) fragments were continuously monitored during the analysis.

2.3. Catalytic Activity

The vapor-phase conversion of phenol (Sigma-Aldrich, ≥ 99.0%) was carried out in a fixed-bed quartz reactor at atmospheric pressure and 330 ºC. Prior to the reaction, the catalyst was treated *in situ* under pure hydrogen (60 mL min^{-1}) (Air Products, 99.999 %) at 360 ºC (10 ºC min^{-1}) for 1 h. The reactant mixture was obtained by flowing H_2 through the saturator containing phenol, kept at the specific temperature required to obtain the desired H_2/phenol molar ratio (about 60). The bulk samples were diluted with inert material (SiC mass/catalyst mass = 12) to avoid the hot-spot formation and to keep the catalytic bed volume constant. The initial phenol conversion was taken after 10 min of time-on-stream (TOS) to avoid the possible influence of coke formation. All lines were heated at 250 ºC to prevent product condensation. The reaction products were analyzed by gas chromatography using a GC Shimadzu (GC-2014), equipped with an HP-Innowax capillary column and a flame-ionization detector (FID). The product yield, selectivity for each product, and the HDO rate were calculated as follows:

$$Product\ yield\ (\%) = \frac{mol\ of\ product\ produced}{mol\ of\ phenol\ fed} \times 100$$

(Equation 3)

$$Selectivity\ (\%) = \frac{mol\ of\ product\ produced}{mol\ of\ phenol\ consumed} \times 100$$

(Equation 4)

$$HDO\ rate\ (mol\ min^{-1} g_{cat}^{-1}) = \frac{yield\ of\ deoxygenated\ product\ (Benzene) \times\ F}{Mo\ loading\ \times catalyst\ mass\ (g)}$$

(Equation 5)

where F means the molar flow rate (mol min^{-1}) of phenol.

To compare the performance of the different catalysts, site time yield (STY) was calculated from redox-active Mo species (determined by equations 1 and 2), as follows in equation 6.

$$STY\ (h^{-1}) = \frac{molar\ flow\ rate\ of\ HDO\ product\ (Benzene)\ formed}{mols\ of\ redox\ active\ Mo\ species}$$

(Equation 6)

The deactivation profiles were calculated using the equations 7, 8, and 9, applying the first-order decay kinetic model [11].

$$a(t) = \frac{-r_{A_t}}{-r_{A_0}} = \frac{rate\ of\ reaction\ A\ at\ any\ time}{rate\ of\ reaction\ A\ with\ fresh\ catalyst}$$

(Equation 7)

For first-order decay:

$$a(t) = \exp(-K_d\ t)\ , \qquad \text{where} \quad a(t) = C \ln\left(\frac{1}{1-x}\right)$$

(Equation 8)

Combining the equations (7) and (8):

$$\ln\ln\left(\frac{1}{1-x}\right) = -k_d t + \ln C$$

(Equation 9)

Where *x,* k_d, and *t* mean conversion, first-order deactivation rate constant, and time, respectively.

3. Results and Discussion

3.1 Catalyst Characterization

Table 1 summarizes different structural results of the bulk and carbon-supported samples including elemental composition, crystallite sizes**,** and reducibility. The amounts of

molybdenum and copper were determined by ICP-OES. For the supported samples, the Mo loading was close to the values expected theoretically (13 % wt.), suggesting that loss of molybdenum was negligible during the impregnation procedure. About Cu loadings, a lower Cu/Mo molar ratio (expected= 0.1) than expected was observed for CuMo (0.06), while the experimental value was closer to the theoretical one for CuMo/C (0.09).

The specific surface area of activated carbon (715 $m^2 g^{-1}$) and its related supported catalysts, Mo/C (473 $m^2 g^{-1}$) and CuMo/C (362 $m^2 g^{-1}$), were determined. Results show that the incorporation of molybdenum and the subsequent addition of copper resulted in a decrease in specific surface areas, suggesting a partial blockage of the pores of the support. However, the range of surface areas observed for both Mo/C and CuMo/C systems are, approximately, of the same order showing that the role of surface area, if any, remains limited here.

Fig. 1 shows the X-ray diffractograms of bulk and carbon-supported calcined catalysts. The XRD pattern of the bulk molybdenum oxide sample only exhibits peaks related to the orthorhombic MoO_3 phase (2θ (plan) = 23.3º (110); 25.7º (040) and 27.3º (021); JCPDS 05-0508), while the diffractogram for bulk CuMo also shows characteristic reflections of the triclinic $CuMoO_4$ phase (2θ (plan) = 22.4º (-211); 23.2º (0-12); 23.9º (201) and 26.5º (-202); JCPDS 22-0242) (Fig. 1B).

Table 1. Elemental composition, crystallite size of samples, and TPR analysis.

Sample	Mo	Cu	Cu/Mo	Crystallite size (nm)[a]						Reduction[b]	
				Calcined samples			Samples treated with H_2 at 360 ºC			T_{peak}	Transformations
	(wt. %)		(molar ratio)	d_{MoO3}	d_{MoO2}	d_{Cu}	d_{MoO3}	d_{MoO2}	d_{Cu}	(ºC)	
MoO_3	—	—	—	56	—	—	45	—	—	674	$MoO_3 \Rightarrow MoO_2$
										699	$MoO_2 \Rightarrow Mo$
CuMo	64.5	2.7	0.06	165	—	—	—	33	—	326, 367 and 415	$CuMoO_4$ transformations (Equation 12)
										652	$MoO_3 \Rightarrow MoO_2$
										715	$MoO_2 \Rightarrow Mo$
Mo/C	12.7	—	—	—	24	—	—	24	—	400	Reduction of MoO_3 octahedral
										607	Reduction of MoO_3 tetrahedral
CuMo/C	13.0	0.76	0.09	—	21	—	—	21	—	389	Reduction of MoO_3 octahedral
										591	Reduction MoO_3 tetrahedral
Cu/C	—	*	—	—	—	32	—	—	19	150	$CuO \Rightarrow Cu_2O$
										320	$Cu_2O \Rightarrow Cu^0$
										601	Reduction of oxidized carbon

[a] Crystallite size of Mo and Cu calculated using the Scherrer equation considering the MoO_3 (040) plane ($2\theta = 25.7º$) for bulk samples, and the MoO_2 (-111) plane ($2\theta = 26$ º) and Cu (111) plane ($2\theta = 43.3$ º) for carbon-supported samples.
* Not done.
[b] TPR analysis (Fig. 4).

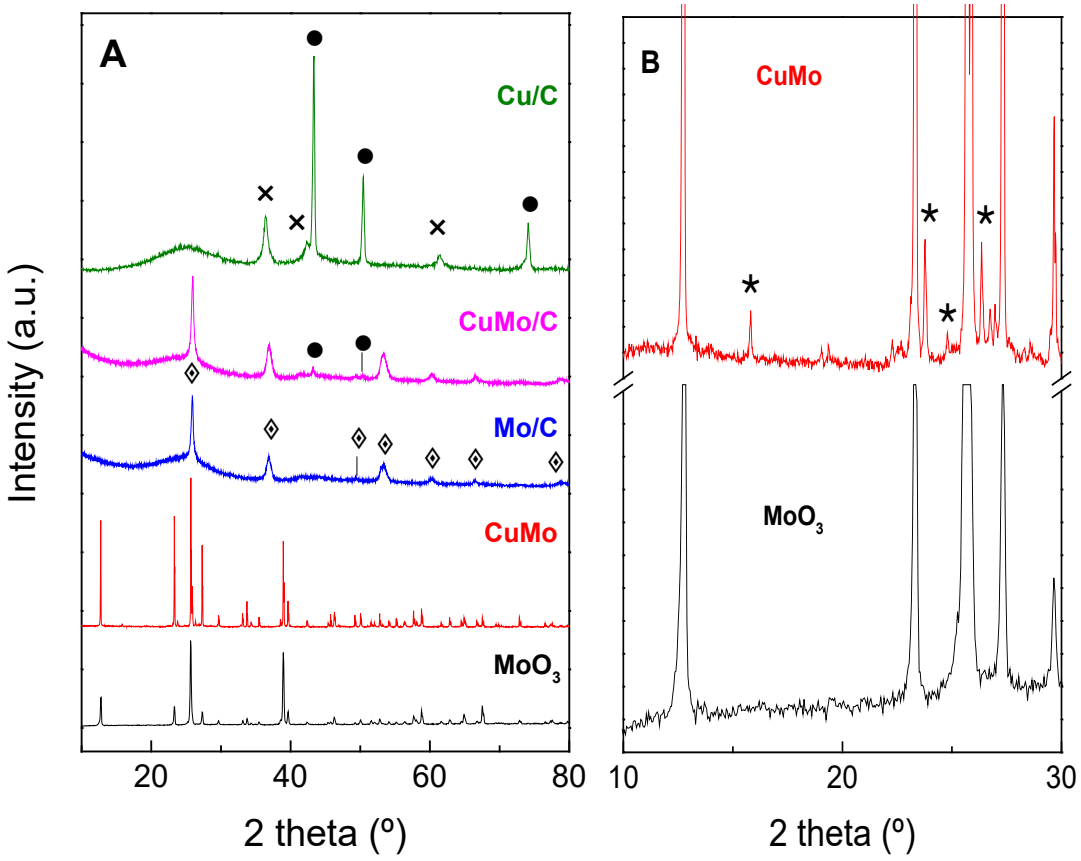

Fig. 1. X-ray diffractograms of the calcined samples: (A) $10 < 2\,\Theta < 80°$; (B) $10 < 2\Theta < 30º$. [(◈) MoO_2, (●) Cu^0, (✕) Cu_2O and (✶) $CuMoO_4$]

The XRD pattern of activated carbon (not shown) displays two broad diffraction peaks around 25 and 43º attributed to amorphous carbon and graphitic structures [27,28]. Moreover, the diffractograms of carbon-supported samples, Mo/C and CuMo/C, also exhibit diffraction peaks characteristic of the MoO_2 plane (2θ (plan) = 26º (-111); JCPDS 32-0671) while the Cu(0) metallic phase (2θ (plan) = 43.2º (111) and 50.3º (200); JCPDS 04-0836) was also observed on the XRD pattern of CuMo/C.

The diffractogram of Cu/C exhibits peaks at 36.3, 42.3, and 61.5º (JCPDS 05-0667), 111, 200, and 220 plans, respectively, related to Cu_2O while contributions observed at 43.3, 50.4, and 74.1º (JCPDS 04-0836), 111, 200, 220 plans, respectively, are related to metallic copper. The presence of these two phases indicates that Cu(II) species were wholly reduced in this case either to Cu(I) or Cu(0) when supported on activated carbon and following a

thermal treatment under N_2 atmosphere. Similar behavior was noted by Zhu et al. [29] and Zhang et al. [30]. Furthermore, as Zhu et al. reported, reduced copper species were detected by EXAFS for Cu/C catalysts treated in an inert atmosphere (Ar) at temperatures above 250 ºC, while metallic Cu was the dominant species after treatment at 450 ˚C [29].

XRD results, therefore, suggest that the thermal treatment of carbon-supported samples promoted the reduction of both molybdenum and copper species. It was previously observed that the presence of the MoO_2 phase over activated carbon occurs by auto-reduction of ammonium heptamolybdate (Equation 10) [20,21,31,32].

$$3\ (NH_4)_6Mo_7O_{24} \rightarrow 21\ MoO_2 + 30\ H_2O + 7\ N_2 + 4\ NH_3 \quad \text{(Equation 10)}$$

Kirakosyan and coworkers [33]studied the thermal treatment of binary and ternary mixtures of MoO_3, CuO, and carbon black in an argon flux. They observed a similar behavior to the one found here. In this respect, the formation of $CuMoO_4$ from a mixture of MoO_3 and CuO under thermal treatment at 470°C – 650 ºC was also obtained. However, it should be noted that in their study, the thermal treatment was carried out under argon flow versus helium in our case. They also observed that the presence of carbon induced the reduction of Mo (VI) and Cu(II) to Mo (IV) and Cu (I) and Cu (0), respectively, with CO and CO_2 release, in the binary compositions MoO_3 + C and CuO + C. They also tested a ternary mixture (MoO_3 + CuO + C) and found that in the 550 – 640 ºC temperature range, the following reaction occurs:

$$MoO_3 + CuO \rightarrow Cu_6Mo_5O_{18} + Cu^0 + MoO_2 \quad \text{(Equation 11)}$$

The crystallite size of Mo was estimated by the Scherrer equation using the diffraction peaks of MoO_3 at $2\theta = 25.7^o$ ((040) plane) for bulk samples and diffraction peaks of MoO_2 at $2\theta = 26.0^o$ (MoO_2 (-111) plane) and/or metallic Cu at $2\theta = 43.3^o$ (Cu^0 (111) plane)

for supported samples. The values of crystallite sizes are also reported in Table 1. As can be noted, the bulk catalysts showed a significant difference in MoO_3 crystallite size after adding Cu (d_{MoO3} for CuMo catalyst was three times higher than for MoO_3 catalyst, 165 nm vs 56 nm) whereas no noticeable differences can be noticed with carbon-supported catalysts. Indeed, for carbon-supported catalysts (Mo/C and CuMo/C), the addition of copper did not change the MoO_2 crystallite size (21-24 nm). These results could be related to the high surface area of activated carbon that may allow a higher dispersion and better stabilization of molybdenum oxide species.

The X-rays diffractograms of samples treated with H_2 at 360 ºC for 1 h, labeled as MoO_3_H_2, CuMo_H_2, Mo/C_H_2, and CuMo/C_H_2, are shown in Fig. 2. The MoO_3_H_2, even after H_2 treatment, still exhibits the characteristic diffraction peaks of MoO_3 whereas CuMo_H_2 shows a drastic change with only peaks of MoO_2 without detection of a copper metallic phase. For the carbon-supported catalysts, MoO_2 is still observed over Mo/C_H_2 and CuMo/C_H_2. However, for copper species, only the metallic Cu phase is observed this time for CuMo/C_H_2 and Cu/C_H_2. Moreover, as shown in Table 1, the treatment with hydrogen did not cause any significant change in crystallite size, except for CuMo with a drastic decrease consecutively to the formation of MoO_2.

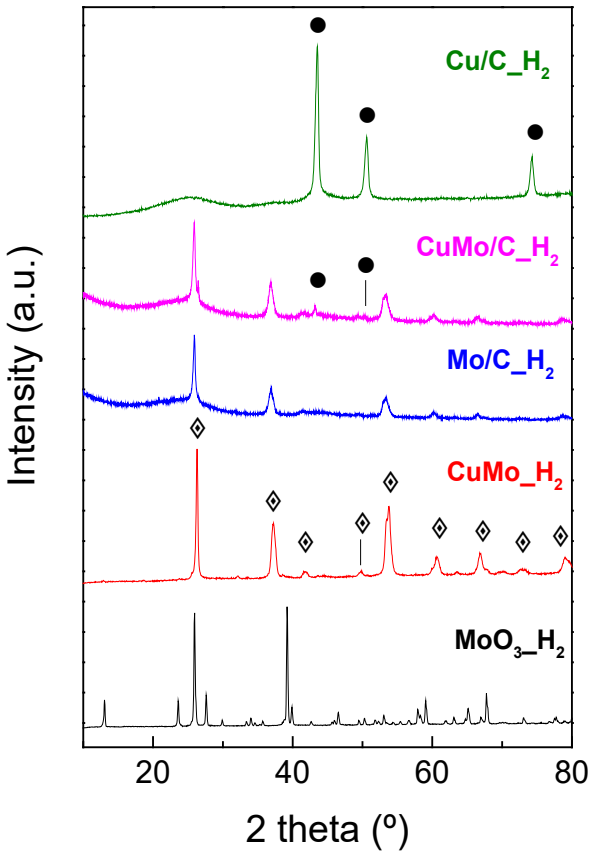

Fig. 2. X-ray diffractograms of the samples treated with H_2 [(◈) MoO_2 and (●) Cu^0].

XPS analyses were carried out to determine the surface chemical composition of the catalysts and the oxidation states of the elements present, allowing the determination of the proportions of molybdenum and copper species at different oxidation states present on the catalyst surface. In this respect, XPS also allows estimating the relationship between the surface and bulk composition and therefore surface enrichment in a given element. Table 2 lists the proportion of Mo and Cu species present on the surface of the calcined samples (at 500 ºC for 3 h, under air flow (unsupported sample) or N_2 flow (supported samples)) and the treated samples (calcined samples treated at 360 ºC for 1 h, under H_2 flow).

CuMo showed almost 100 % Mo (VI) (Fig. S1), indicating that the addition of copper did not modify the oxidation state of molybdenum after calcination treatment. Furthermore, the carbon-supported samples (Mo/C and CuMo/C) presented Mo(IV), Mo(V), and Mo(VI) species (even after calcined under N_2 flow) with a predominance of Mo(VI) entities in

contrast with the XRD analysis in which only MoO_2 species were observed (Fig. S1). XPS being a superficial technique, these results strongly suggest that the surface of these samples may have been oxidized into MoO_3, leading to a MoO_2@MoO_3 conformation, as was previously reported by Ansaloni et al. [21].

Table 2. Proportions of the Mo and Cu species present on the surface of the samples and respective binding energies as determined by decomposition of XPS Mo $3d_{5/2}$ and Cu $2p_{3/2}$ core level spectra of different catalysts.

Sample	Species proportions (%)					
	Mo IV[a]	Mo V[a]	Mo VI[a]	Cu I[a]	Cu II[a]	x (MoO_{3-x})[b]
MoO_3_H_2	8	36	56	—	—	0.3
CuMo	—	2	98	32	68	0
CuMo_H_2	14	19	67	71	29	0.2
Mo/C	7	9	84	—	—	0.1
Mo/C_H_2	9	24	67	—	—	0.2
CuMo/C	26	31	43	88	12	0.4
CuMo/C_H_2	18	23	59	67	33	0.3

[a] Binding energy of Mo and Cu states: Mo IV (229.8 ± 0.3 eV); Mo V (231.6 ± 0.5 eV); Mo VI (232.8 ± 0.2 eV); Cu I (932.8 ± 0.4 eV) and Cu II (934.8 ± 0.4 eV [34–36]
[b] x was calculated using the formula (MoO_{3-x}), using the mean oxidation state of Mo [37].

The addition of Cu to Mo/C modified the relative proportion of the molybdenum species on the surface of the samples, with the Mo (VI) amount decreasing from 84 to 43 % (Fig. S1). These data indicate that carbon support played a crucial role in reducing molybdenum. At the same time, the addition of copper tends to amplify this phenomenon, in agreement with the previous studies by Thomazeau et al. [31] [31]and Kirakosyan et al. [33]. The bimetallic samples displayed the presence of two different copper species (Fig. S2), Cu (I) (Auger parameters around 1849 eV) and Cu (II) (Auger parameters around 1851 eV [34,37]. The CuMo sample presented almost 70 % of Cu(II) while the proportion of Cu

species present on the surface of CuMo/C was quite different (88 % of Cu(I) and 12 % of Cu(II)), indicating that in the presence of activated carbon, copper was reduced during the calcination under N_2. No signal of Cu (0) was observed by this technique. In contrast to these results, the XRD patterns (Fig. 1) showed different Cu species for both catalysts. So, the sample surface was once again oxidized and the structure $Cu@Cu_2O$ may have been formed.

Concerning the catalysts treated with hydrogen ($MoO_3\_H_2$, $CuMo\_H_2$, Mo/C_H_2, and $CuMo/C\_H_2$), Fig. S3, S4, and S5, as expected, the treatment generally promoted an increase in the concentration of species with lower oxidation numbers. Furthermore, this reduction process was less pronounced in samples containing copper. On the other hand, the treatment with H_2 of the CuMo/C sample increases the concentration of species with the highest oxidation state, Mo (VI) and Cu (II). In this case, the C support helps to improve the Cu-Mo interaction. The lower concentration of Mo (VI) and Cu (II) species for the CuMo/C sample (without H_2 treatment) should be explained due to the reducing effect of the carbon support. In this case, carbon gives electrons to Cu, which transfers them to Mo. Transferring electrons to Mo helps part of Cu(0) to go back to the metastable Cu(I) oxidation degree leading to a subtle equilibrium between C, Cu, and Mo. If an H_2 treatment is applied to $CuMo/C\_H_2$, this equilibrium is broken: the hydrogen treatment then limits the role of carbon as a reducing agent since the support is probably first partly reduced by the hydrogen supply. Direct electron transfers between C, Cu, and Mo are therefore restrained, hampering the ability of Cu and Mo to be present at lower oxidation degrees.

Regarding the binding energies, should be noted that there was no significant variation in the binding energy at 531.5 eV relative to the O 1s core level spectra (Fig. S5), hampering our ability to use this signal to determine the presence or not of oxygen vacancies. This observation was also made by Zhang et al., with even much higher copper loading (13 % wt) [37]. Nevertheless, based on the respective proportions of the different molybdenum

species (Mo (IV), Mo (V), and Mo (VI)) found in our samples, mean oxidation states can be determined, revealing in this way the presence of non-stoichiometric molybdenum oxide entities and the existence of oxygen vacancies [37]. As shown in Table 2, the concentration of oxygen vacancies in the samples follows the subsequent order: CuMo (0) < Mo/C (0.1) < CuMo_H_2 (0.2) ≅ Mo/C_H_2 (0.2) < MoO_3_H_2 (0.3) ≅ CuMo/C_H_2 (0.3) < CuMo/C (0.4). Therefore, these results emphasize a quite different role of copper depending on the presence or not of carbon support: if we assume the approach proposed by Zhang et al. [37], while for unsupported samples, the addition of Cu does not affect the number of oxygen vacancies present on the surface, on the contrary, for carbon-supported samples, copper helps to promote the formation of oxygen vacancies.

Raman spectroscopy was used to detect any local change within dispersed molybdenum oxide domains by probing the Mo-O vibrational modes of all samples and identifying the Mo and Cu phases presented in the samples. Fig. 3 shows the Raman spectra of the calcined samples (spectral region between 200 – 1200 cm^{-1}).

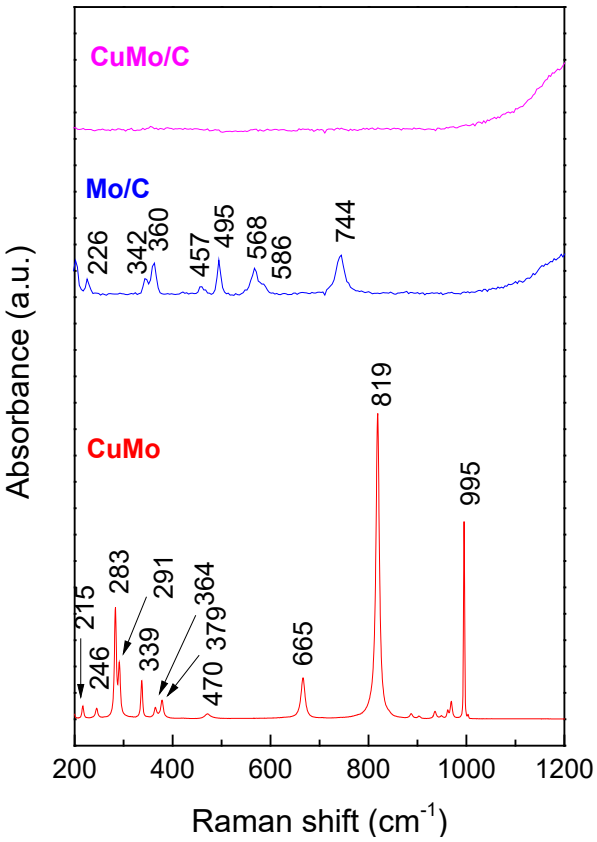

Fig. 3. Raman spectra of calcined samples.

In agreement with XRD results, Fig. 1, the sample CuMo presents bands related to the MoO_3 vibrations (995, 819, 665, 470, 379, 364, 339, 291, 283, 264, and 215 cm^{-1}) [38,39]. Besides the MoO_3 bands, this sample also shows bands between 860 and 980 cm^{-1}, Fig. S6. These bands (887, 903, 936, 949, 962 cm^{-1}) can be assigned to the presence of $CuMoO_4$ (species shown in XRD) [40]. As for carbon-supported samples, bands associated with MoO_2 were observed only in the Mo/C spectrum (226, 342, 360, 457, 495, 568, 586**,** and 744 cm^{-1}). Note that Raman spectroscopy did not detect any Mo phase for the CuMo/C spectrum, Fig. 1. In addition, Cu_xO signals were not detected in CuMo/C, suggesting that the quantity of copper added was not enough to create copper oxides or that the dispersed copper species must be Raman-inactive [41].

Fig. S7 shows the Raman spectra of carbon-supported samples in a broader spectral region (300 – 3500 cm^{-1}). It can be seen that all the samples showed bands related to the

graphitic structure at 1600 cm^{-1} and 1336 cm^{-1}. The band localized at 1600 cm^{-1}, called G-band, which is common to all sp^2 carbon systems, is related to the stretching of the C-C bond in graphitic materials. The band localized at 1336 cm^{-1}, called D-band, is related to the crystalline structural disorder, that is, the presence of defects such as curvatures, amorphous carbon (sp^3 hybridization), openings, and bifurcations [42]. Quantifying disorder in a carbon material is usually made by analyzing the intensity ratio (I_D/I_G) between the disorder-induced D-band and the Raman-allowed G-band. Both samples showed the same ratio, around 0,9, so the introduction of Cu did not change the structure of the activated carbon.

TPR was used to investigate the reducibility of the calcined samples. The reduction profile of each sample is shown in Fig. 4, and the main temperature/transformations observations in each profile are summarized in Table 1. For MoO_3, the TPR profile shows two reduction peaks, at 674 ºC and 699 ºC, suggesting the existence of two different environments, possibly related to some differences in molybdenum coordination. These transformations are also observed in the CuMo reduction profile (652 and 715 ºC). Besides, three peaks centered at around 326, 367, and 415 ºC can be assigned to various transformations of copper molybdate as observed by Wen et al. and Soltys et al. [43,44] and shown in Equation 12.

$$CuMoO_4 \rightarrow Cu_{4-x}Mo_3O_{12} \rightarrow Cu_4Mo_5O_{17} + Cu_6Mo_5O_{18} \rightarrow MoO_2 + Cu$$

(Equation 12)

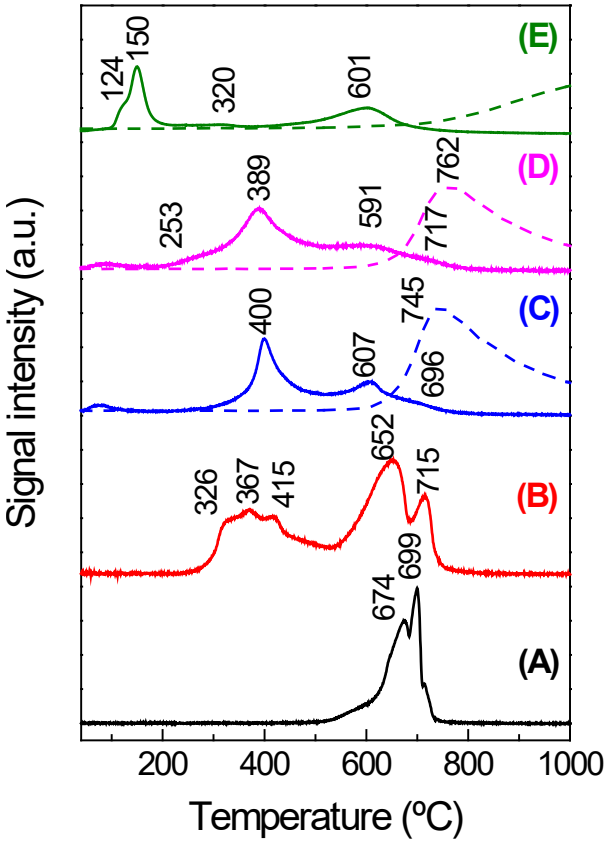

Fig. 4. H_2-TPR profile of bulk and supported samples: (A) MoO_3, (B) CuMo, (C) Mo/C, (D) CuMo/C and (E) Cu/C [(—) H_2O (m/z =18) and (---) CH_4 (m/z =15) release].

The TPR of activated carbon (Fig. S8) and all the carbon-supported catalysts presented water release of around 590 ºC, which may be related to the reduction of oxidized surface carbon and gasification of carbon into CO, as previously reported [21,30,45,46]. In addition, signals of CH_4 (m/z = 15) (dashed lines) and CO (m/z=28) (not shown) release were also observed ratifying these affirmations.

The TPR of Mo/C shows two peaks of water release with the maximum at 400°C and 607ºC and one shoulder at 696ºC, whereas CuMo/C exhibits two prominent peaks at 389°C and 591ºC and one shoulder at 717ºC. For both catalysts, the first peak can be assigned to the reduction of octahedral MoO_3 species, while the second can be assigned to the reduction of tetrahedral MoO_3 species. The oxidized carbon on the surface, while the highest temperature peak (shoulder) is related to molybdenum carburization due to the reduction of

surface carbon [32,46]. Although XRD did not indicate the presence of Mo (VI), the XPS results show that there is MoO_3 on the surface of this catalyst, as also observed by Cai et al. and Ansaloni et al. [20,21]. CuMo/C sample still presents a shoulder at approximately 285 ºC, probably related to the reduction of CuO and Cu_2O to metallic Cu, dispersed on the support surface as suggested by the XPS results. The release of methane was also observed for the carbon-supported samples, Fig. 4 (dashed lines), suggesting that the reduction of activated carbon starts over 550 ºC.

The TPR profile of Cu/C showed three peaks, the first peak, around 124 ºC, can be attributed to the reduction of CuO highly dispersed on the surface, and another with a maximum at 150 ºC, assigned to the reduction of Cu_2O (observed by XRD), in greater quantity, and the third peak at 601 ºC related to the reduction of oxidized carbon on the surface and gasification of carbon support into CH_4 and CO, ratifying by their signals observed by mass spectroscopy (the latter not shown) [30]. The reducibility of bulk CuO (Fig. S8) was analyzed under the same conditions, and its profile exhibited just one peak with a maximum at 179 ºC, indicating the direct reduction of Cu(II) to Cu(0). This behavior suggests that, in the presence of carbon, the reduction proceeds in two stages, modifying the proportion of formed species.

The higher reduction temperature of copper species on the molybdenum samples indicates a strong interaction between Cu and Mo, ratifying our observations based on XPS results. According to Zhu et al., the Cu-Mo interaction forms a stable, coordinated structure that is difficult to reduce [47]. Then, the TPR data agree with the XPS and XRD results of H_2-treated samples. It is possible to note that the species observed for the samples treated with H_2 at 360 ºC are consistent with the transformations during the TPR analyses described in Table 1.

The O_2 chemisorption and H_2O-TPD techniques were also used to determine the concentration of oxygen vacancies on the bulk and supported samples. In addition, oxygen chemisorption was performed to evaluate the ability of catalysts to capture oxygen in catalytic test reaction conditions, thus determining the amount of available active sites, possibly oxygen vacancies, and then relating these results to those obtained with phenol deoxygenation.

According to the oxygen chemisorption profiles (Fig. 5), it is possible to observe that the bulk catalysts present a rapid increase in chemisorbed oxygen uptake, reaching a constant level at low pressures (about 50 mmHg). In comparison, samples containing activated carbon show a gradual increase in oxygen chemisorption without achieving stability.

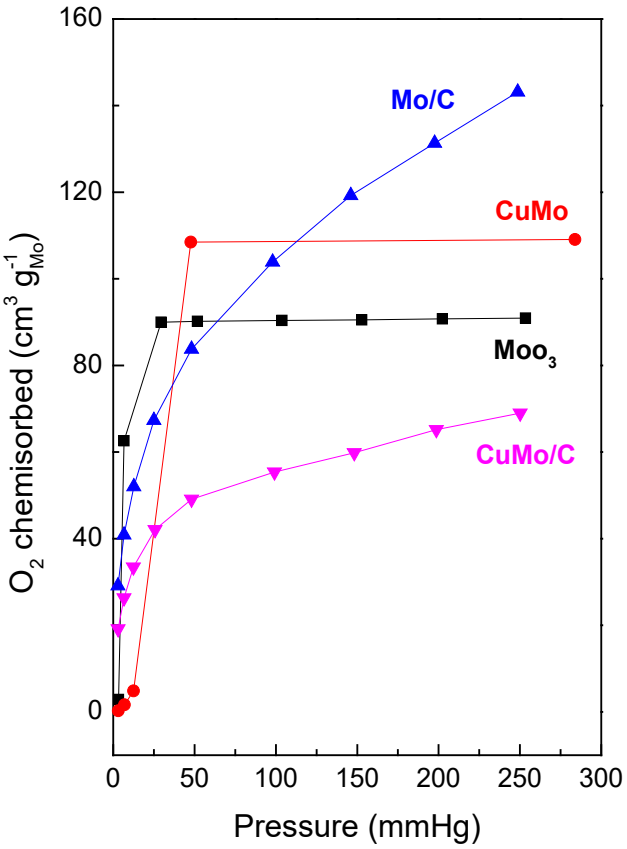

Fig. 5. O_2 chemisorption isotherms of samples at 350 ºC.

The result shows that the oxygen captured by CuMo (108 cm^3 g_{Mo}^{-1}) was slightly higher than that of MoO_3 (90 cm^3 g_{Mo}^{-1}), consequently, the quantity of active Mo-redox

(determined by equation 2) was 92 and 76 %, respectively. Therefore, it is possible to perceive that adding copper to the bulk MoO_3 promoted the capture of oxygen. However, this technique was not able to determine the number of oxygen vacancies present in supported ones, probably due to the slow diffusion of oxygen into the pores of the support, and it can be difficult to reach saturation at low pressures. Therefore, this type of experiment is not appropriate in our case to determine the total amount of chemisorbed oxygen.

Fig. 6 depicts the H_2 (m/z = 2) profiles of H_2O-TPD of the Mo-based samples. The H_2O-TPD analysis allows to determine the number of anionic vacancies present on the surface of oxides. This measure is related to the ability of some solids to dissociate water molecules that are adsorbed on the catalyst surface [26,48]. The adsorption of H_2O on the oxide surface generates hydroxyl species (OH(a)), which can undergo two competing pathways: (i) the association of OH(a), releasing H_2O with the production of oxygen vacancies ($OH(a) + OH(a) \rightarrow H_2O(g) + O_{lattice} + O_{vacancy}$) and another for which (ii) H_2 is formed, ($OH(a) + OH(a) \rightarrow H_2(g) + 2O_{lattice}$). So, the H_2 formation would be related to the presence of oxygen vacancies. As can be observed, all the samples exhibit a similar profile of H_2 desorption, with just one peak around 400 ºC, suggesting that they present the same type of active sites, although with different relative amounts.

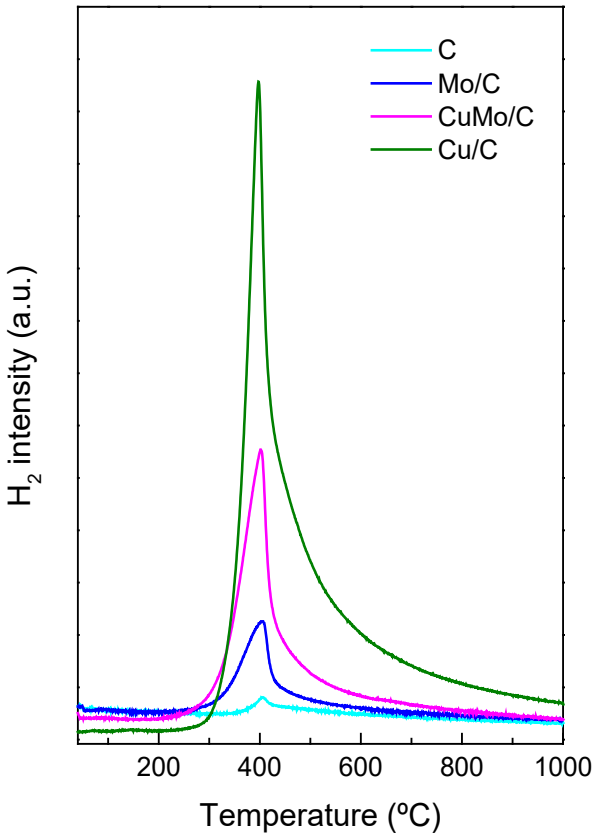

Fig. 6. H_2 (m/z=2) spectra of H_2O-TPD profiles of the samples (0.2 g, 360 ºC (10 ºC min^{-1}), 1 h.

Considering results normalized to Mo amount, it is possible to realize that the quantity of H_2 per gram of Mo generated by CuMo/C (211 µmol H_2 g_{Mo}^{-1}) was almost three times greater than Mo/C (81 µmol H_2 g_{Mo}^{-1}), which suggests that the majority of oxygen vacancies have been generated through the addition of copper in CuMo/C, as also speculated by Kasiraju & Grabow [25].

Some authors have reported that metallic Cu (whose presence was observed by XRD) [49–51] is an active site for the H_2O dissociation. It was observed that Cu/C (72.3 µmol $H_2.g_{cat}^{-1}$) generated more hydrogen than Mo/C (10.8 µmol H_2 g_{cat}^{-1}) and CuMo/C (28.1 µmol $H_2.g_{cat}^{-1}$), so Cu would be catalyzing the decomposition of water. However, the amount of copper in CuMo/C is only 1% (w/w), whereas the amount of copper in Cu/C is 13 % (w/w), showing that in CuMo/C, the contribution coming from copper is not significant.

3.2 HDO of phenol over molybdenum catalysts

Table 3 compares the results of phenol conversion for the HDO reaction performed at 330 ºC at atmospheric pressure on an equivalent Mo mass basis. Results are expressed considering the HDO reaction rate of bulk and supported molybdenum catalysts. In addition, the effect of the pre-treatment with H_2 at 360 ºC was also evaluated. The amount of benzene produced was greater than 98 % for all molybdenum-based-catalysts, while Cu/C provided a selectivity of 50 % to benzene, 24 % to cyclohexene, and 26 % to cyclohexanone.

Table 3. Catalyst activity in phenol HDO.

Sample	Conversion (%)		HDO rate (mol min^{-1} g_{Mo}^{-1})	
	No treatment	H_2 treatment at 360 ºC	No treatment	H_2 treatment at 360 ºC
MoO_3	0.5	1	0.001	0.002
CuMo	1.1	11	0.002	0.024
Mo/C	1.2	16	0.003	0.034
CuMo/C	7	28	0.015	0.059
Cu/C	1	2	0.001	0.002

Reaction conditions: T = 330 ºC, P = 0.1 MPa, TOS = 10 min, WHSV = 11.7 h^{-1}.

As shown in Table 3, without the hydrogen treatment, all catalysts exhibited very low phenol conversion (around 1 %) except for CuMo/C, which reaches 7 %. Therefore, it is possible that, under these conditions, neither the support nor the addition of copper significantly affected the activity. However, the activity tends to increase when carbon and copper are combined. The Cu_xO species present on Cu/C are not active, but when deposited on the surface of the MoO_x catalysts, copper promotes modifications by removing electronic

density from the surface of covalent bonding oxides, probably due to the hybridization of metal d-orbitals and oxygen p-orbitals. This interaction promotes charge transfer processes at the metal-oxide interface, facilitating the removal of some oxygen atoms and enabling the generation of oxygen vacancies [52–55].

The hydrogen treatment significantly affects the catalytic activity, which follows the order: MoO_3 ≈ Cu/C < CuMo < Mo/C < CuMo/C. According to this result, it can be inferred that the support and/or the addition of copper favored phenol conversion. Moreover, the temperature employed for the treatment of the catalysts before the catalytic tests (360 ºC) is lower than the reduction temperature of the molybdenum species (around 400 ºC), as seen in Fig. 2. Therefore, the heat treatment helps to produce more oxygen vacancies that are considered the active sites for the hydrodeoxygenation of aromatic compounds without modifying the support. This result is consistent with the literature, in which the presence of reduced Mo species (Mo (IV) and Mo (V)) has been shown to increase the activity of catalysts [56,57].

The HDO reaction rate results at low phenol conversion are listed in Table 3. CuMo/C is the most active for HDO with or without the hydrogen treatment among the studied catalysts. The rate of deoxygenation followed the order: MoO_3 (0.001) ≈ Cu/C (0.001) < MoO_3_H_2 (0.002) ≈ CuMo (0.002) ≈ Cu/C_H_2 (0.002) < Mo/C (0.003) < CuMo/C (0.015) < CuMo_H_2 (0.024) < Mo/C_H_2 (0.034) < CuMo/C_H_2 (0.059). This evolution shows a correlation between the HDO reaction rate, and the number of oxygen vacancies created by adding copper. At the same time, carbon support and MoO_2 species are also two important parameters. If normalizing the performance of different bulk catalysts based on redox-active Mo species, the initial site time yields (STY) of MoO_3 and CuMo were 0.16 h^{-1} and 1.47 h^{-1}, respectively. These results indicate that the addition of copper increased the

intrinsic activity of the redox-active Mo species, enhancing the catalyst activity without affecting the selectivity in benzene.

Under the studied reaction conditions, bulk samples display activity inferior to carbon-supported catalysts, indicating that the higher dispersion of the Mo species could be relevant to the activity or that MoO_2 species supported on carbon, as shown by XRD profiles, are more active than MoO_3 entities.

In the literature, many works were based on molybdenum oxides as catalysts for the hydrodeoxygenation of biomass-derived compounds. However, controversial results were found concerning the role played by the different Mo species. Several authors affirm that the partially reduced MoO_3 presents high activity and selectivity to the cleavage of the C-O bond since it contains active sites associated with the presence of oxygen vacancies, Mo (V) and Mo (III), Lewis acids, oxide defects, acidic and metallic active sites or subcoordinated Mo [10–12,35,57–63]. According to these authors, the appearance of MoO_2 along the reaction time would reduce the catalytic activity. On the other hand, other works showed that the presence of Mo (IV) in the catalysts provided interesting values in activity and selectivity to deoxygenated products [13,20,21,64]. In all works, MoO_2 was supported over carbon materials (activated carbon, carbon nanotubes) and, according to Sun and co-workers (2005), the activated carbon has been demonstrated to be effective in splitting H_2 into atomic forms [65]. In addition, it has been reported that copper can adsorb and dissociate molecular H_2 [66,67]. Therefore, a synergy between Cu, MoO_2, and the activated carbon may contribute to the formation and activation of hydrogen atoms allowing homogeneous H···H splitting to produce H·, promoting slow deoxygenation of phenol into benzene. This behavior was observed by Liu et al. (2018) [68], that studied the effect of doping MoO_2@C with Co for the hydrodeoxygenation of guaiacol.

The improvement of the conversion (4.0 to 6.2%), keeping constant the selectivity to hydrodeoxygenated molecules, was also observed by Itthibenchapong and collaborators (2021) [69]. They studied the incorporation of copper on the surface of MoO_{3-x}/TiO_2 (Cu/Mo = 0.35 molar ratio) for the deoxygenation of p-cresol in the liquid phase at 300ºC and 5 MPa. According to them, metallic copper effectively promotes H-H dissociation, generating free H atoms. Then, these atoms activate the formation of oxygen vacancies over the MoO_{3-x} surface through a spillover process favoring the HDO route.

As already reported in the literature, copper-based catalysts with different supports (activated carbon, carbon nanotubes, TiO_2, and ZrO_2) containing 2-5 wt. % Cu loading were tested in the deoxygenation of aromatic compounds (phenol, guaiacol, eugenol) at diverse reaction conditions (liquid and gas phases, 260 – 450 ºC, atmospheric pressure – 5 MPa). However, these catalysts showed low activity in HDO (0 – 5.3 % conversion) [32,70–73]. In the present study, the Cu/C catalyst showed low catalytic activity for HDO (2 %) and selectivity for benzene (50 %). Nevertheless, adding copper to the molybdenum oxide catalysts improved the phenol conversion for the bulk and the supported catalysts, thus suggesting that Cu improves the tendency to form oxygen defects over MoO_x, as hypothesized previously by Kasiraju & Grabow (2018) [25]. This effect of copper was confirmed by TPD-H_2O and O_2 chemisorption, which showed an increase in the quantity of H_2 generated and of chemisorbed oxygen, respectively.

Concerning the reaction selectivity, mono and bimetallic molybdenum catalysts produce almost 100 % in benzene, indicating that the addition of copper did not change the selectivity along the direct deoxygenation route (DDO). Furthermore, the calculated STY results of bulk catalysts confirm this observation since MoO_3 (0.16 h^{-1}) shows a low value to CuMo (1.47 h^{-1}), indicating that the addition of copper increased the intrinsic activity of

redox-active Mo species, which enhanced the catalyst activity without affecting the selectivity in benzene.

Two reaction routes are generally proposed for the HDO over bimetallic catalysts composed of an active hydrogenation metal and an oxophilic site: (i) in the presence of oxophilic sites close to the periphery of metal particles, phenol adsorbs as phenoxy species on oxophilic sites of the support; this step is followed by tautomerization and formation of a cyclohexadienone as an intermediate. Then, the carbonyl group is hydrogenated to 2,4-cyclohexadiene, rapidly dehydrating to benzene [74–76]. (ii) The oxygen of the organic compound chemisorbs on the oxygen vacancy of the oxyphilic metal oxides by activating and weakening the C_{Ar}-O bond. At the same time, the metal dissociates H_2 forming hydrides. These hydrides facilitate the rupture of the C-O bond, leading to dehydration [77,78].

Then, based on the literature [68,79], and taking into account the physical-chemical properties and catalytic performance of the studied catalysts, the mechanism represented in Fig. 7 can be proposed: (i) Copper promotes the homolytic cleavage of H_2; at the same time, phenol approaches the oxygen vacancy of MoO_x, and the C_{Ar}-O bond is elongated and weakened. (ii) The H· attacks the C of the C-O bond, which is more susceptible to receiving electrons. (iii) When H· bonds to C, the C_{Ar-O} bond is broken, producing benzene and OH·, which quickly binds to another H· present on the catalyst (probably on the surface of the activated carbon), forming H_2O.

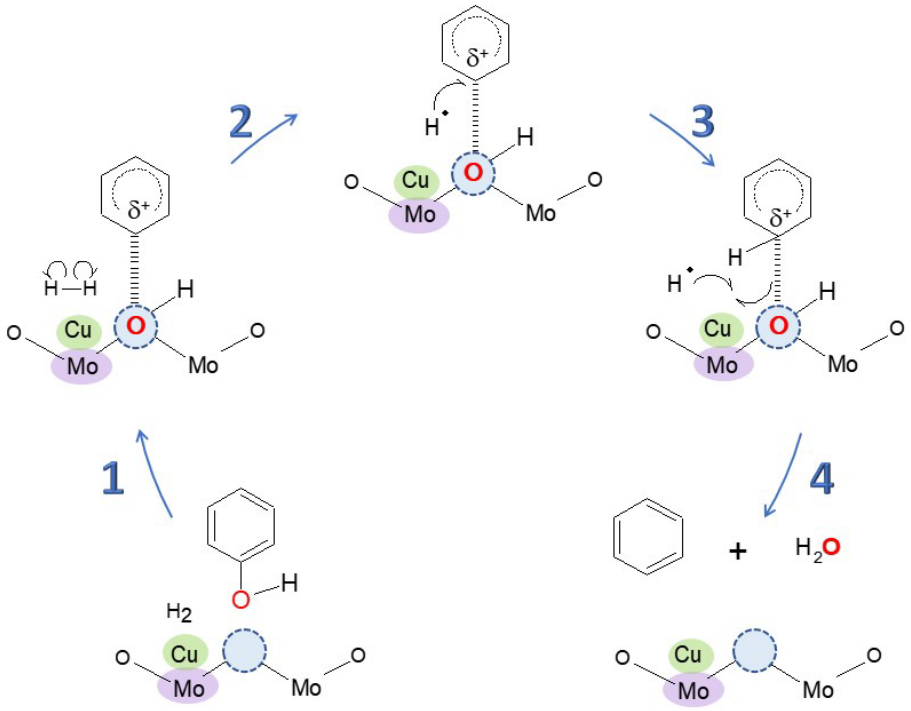

Fig. 7. Proposed mechanism of phenol HDO over CuMo/C.

It can be seen that the order of reducibility of Mo species agrees with the results of TPD-H_2O and the activity of catalysts. Thus, the greater the reducibility of Mo species (higher tendency to create coordinatively unsaturated molybdenum sites), the greater the number of oxygen vacancies, implying an increase in the reactivity of catalysts in HDO. These data agree with what was observed by Shetty et al [12].

3.3 Catalysts deactivation studies

Besides the catalyst activity, its stability is a crucial point to consider in developing catalysts. Catalyst deactivation can occur through different physical (fouling, attrition, crushing, and erosion), thermal (phase transformation and sintering), or chemical (leaching and poisoning) processes [80].

In this work, the catalysts with higher reactivity, Mo/C_H_2, and CuMo/C_H_2, were chosen for stability studies over 6 h under the same experimental conditions. Fig. 8 displays the conversion of the phenol and product distribution as a function of time on stream (TOS) for the catalysts.

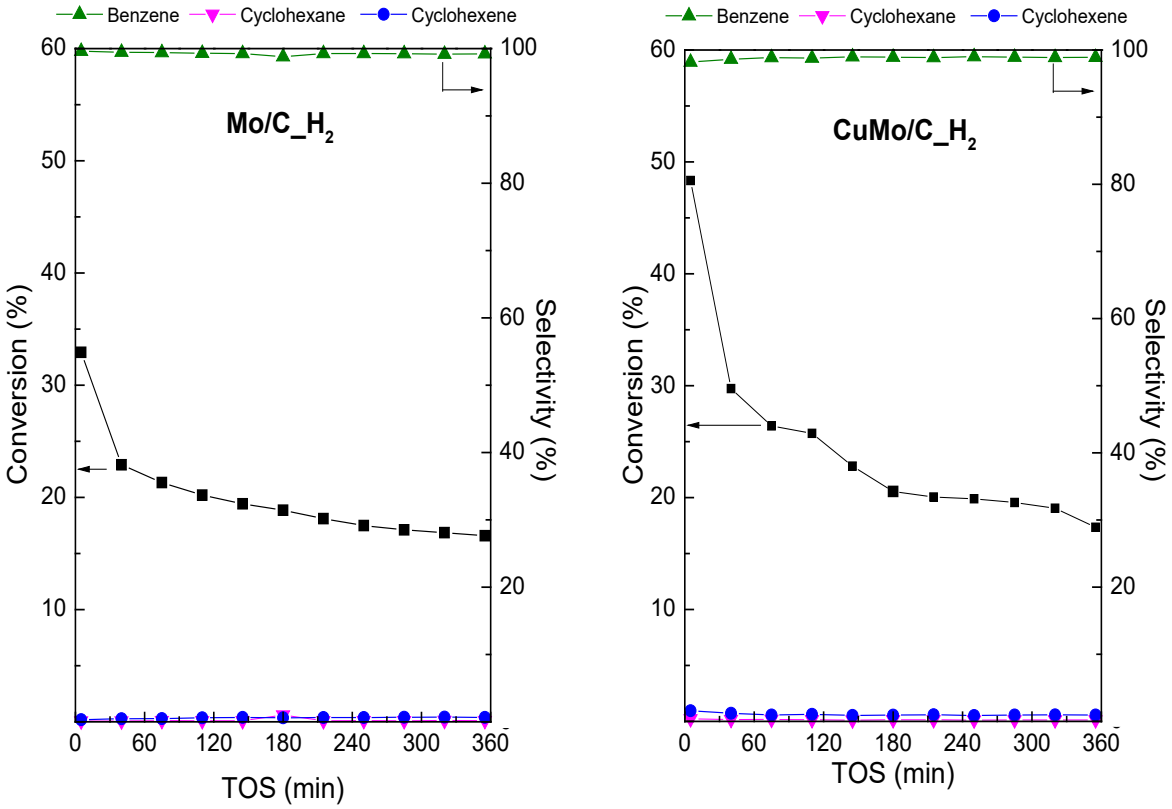

Fig. 8. HDO of phenol with Mo/C_H_2 and CuMo/C_H_2 at 330 ºC (Reaction conditions: 0.1 MPa, $T_{reduction}$ = 360 ºC, WHSV = 5.75 h^{-1}).

For both catalysts, the first-order deactivation profile (Fig. S9) presents three deactivation zones (5 – 45 min, 45 – 180 min, and 180 – 360 min), and the main product observed was benzene (above 98%), which indicates that the selectivity for the cleavage of the C–O bond was maintained throughout the reaction time. For Mo/C_H_2, the phenol conversion decreased from 33 to 17 % with deactivation rate constants 0.01226, 0.00176, and 0.00085 min^{-1}. While for CuMo/C_H_2, the phenol conversion decreased from 48 to 17%, with deactivation rate constants 0.0179, 0.00247, and 0.00114 min^{-1}.

We can see that the first deactivation period (0- 45 min) proceeds quickly, and after that, the deactivation is milder for both catalysts. The fast initial deactivation may be related to the high concentration of active sites at the beginning of the reaction, with the formation of many products that adsorb to the active site, deactivating it.

Agreeing with the literature, the deactivation of catalysts employed at hydrodeoxygenation reaction of aromatic molecules can occur, mainly by the deposition of carbon, sintering, or strong adsorption of the particles [12,81]. This carbon formation can occur by polymerization or polycondensation at the acidic sites of the carbon, blocking the active sites [74,82]. However, the type of carbon formed is related to the composition of the catalytic site and the molecule studied [83,84].

Shetty and collaborators investigated the stability of 10 % MoO_3 dispersed over different supports (SiO_2, γ-Al_2O_3, TiO_2, ZrO_2, and CeO_2) in the hydrodeoxygenation of m-cresol in the gas phase at 320 ºC and 0.1 MPa [12]. According to their results, the supported catalysts were more stable, and the deactivation was attributed to the carbon deposition and the formation of Mo species with low reactivity (e.g., Mo (IV)).

Yu and co-workers (2022) studied the effect of the addition of transition metals (X = Cu, Ni, Cr, Zn, Fe, Co) in the mass ratio X/Mo = 1/10 on the activity of the Mo/C catalyst in the HDO of methyl oleate in liquid phase at 1.0 – 3.5 MPa at 260 – 300 ºC between 1 and 5 h of reaction [85]. Among the metals evaluated, copper provided the best results, keeping the conversion and high selectivity for unsaturated hydrocarbons, 98.8 and 40.2%, respectively. The selectivity to unsaturated products was mainly due to the higher number of oxygen vacancies in CuMo/C. The XRD, XPS, and EPR characterizations indicated that the presence of oxygen vacancies is conducive to the preferential adsorption of carbon-oxygen bonds and prevents the hydrogenation of C=C bonds. Comparing CuMo/C with Mo/C, the former proved to be more resistant to catalyst deactivation, maintaining its

selectivity to unsaturated hydrocarbons. This stability was attributed to the presence of copper, which would preserve the active Mo species through its auto-oxidation. This observation was confirmed by thermogravimetric analysis (in air atmosphere) of the Mo/C and CuMo/C catalysts, which showed that the increase in mass of the Mo/C was 2.26 % against 1.18 % to CuMo/C, suggesting that the insertion of higher copper makes the catalyst less susceptible to oxidation, making CuMo/C more stable than Mo/C. In contrast with our work, the insertion of copper did not increase the stability of the CuMo/C_H_2 catalyst, but rather its activity, seen by the initial conversion values, 48 % versus 33 % for Mo/C_H_2. The difference between the deactivation constants obtained for the first zone (the most drastic one) in each case corresponds exactly to the percentage difference between these conversions (31 %).

De Souza et al (2017) studied the stability of palladium catalysts supported on different materials (SiO_2, Al_2O_3, TiO_2, ZrO_2, CeO_2, and $CeZrO_2$) in the gas-phase HDO reaction of phenol at 0.1 MPa and 300 °C [75]. The authors stated that phenoxy and other intermediate species adsorb strongly on the oxophilic sites, inhibiting further adsorption of the reactants, and concluding that the reduction in the number of the acid sites and the sintering of the Pd particles were the two dominant factors leading to the deactivation of the catalyst. Notably, the catalysts containing TiO_2 and ZrO_2, which have a high oxophilic character, such as molybdenum [86], were more active, directing the reaction towards the deoxygenation of phenol. Moreover, although they deactivated faster than those containing CeO_2 and $CeZrO_2$, the benzene selectivity remained stable and high during the reaction time (20 h).

In the present work, at the end of the 6 h reaction, both catalysts reached the same conversion level (17 %). The selectivity for the deoxygenated product (benzene = 98 % of selectivity) was not changed, indicating that the composition of the active sites was not

modified over the reaction time, maintaining direct deoxygenation as the main route of oxygen removal from phenol. Comparing the diffractograms of fresh and spent catalysts (Fig. S10), it is possible to observe the reduction or disappearance of some peaks related to MoO_2 [2θ (plan) = 26º (-111); JCPDS 32-0671; 37º (-211)] and metallic Cu [2θ (plan) = 50.3º (200); JCPDS 04-0836] phases. This reduction is more pronounced in the CuMo/C_H_2 catalyst, which may explain the greater deactivation of this catalyst (Fig. 8). Based on these results, we can speculate that the deactivation is due to the decrease in the number of available oxygen vacancies in MoO_x phases, which probably is blocked by strong carbon adsorption during the reaction.

4. Conclusion

Bulk and supported molybdenum and copper catalysts were tested in the phenol hydrodeoxygenation in the gas phase at 330 ºC and atmospheric pressure. For bulk samples, copper and molybdenum are found in a mixture of Cu(I) and Cu(II) and Mo(V) and Mo(VI), respectively, whereas on carbon-supported catalysts, copper and molybdenum are present in the Cu@Cu_2O and MoO_2@MoO_3 forms, respectively. For carbon-supported samples, the treatment with nitrogen promotes the reduction of molybdenum Mo(VI) to Mo(IV) and copper Cu(II) to Cu(0). The effect of the support and the copper addition were evaluated. The supported catalysts were more active than the bulks ones, indicating that the presence of MoO_2 species can enhance the activity. The bimetallic catalysts were more active than monometallic ones, suggesting that the incorporation of copper promotes the conversion of phenol because copper would be responsible for: initially relocating the MoOx electronic cloud, promoting the creation of vacancies, and the generation of H•, which promote the cleavage of the C-O bond, previously weakened by oxygen vacancy. The conversion order agreed with the TPD-H_2O method results, suggesting that the H_2 generation represents the

specific sites for hydrodeoxygenation. CuMo/C was the most active among the tested catalysts, with an improvement in the conversion of 1 to 28 % compared to MoO_3, showing good activity at oxygen removal of aromatic oxygenates. This result is probably due to the enhanced formation of surface oxygen vacancies and an optimized cleavage rate of phenol C_{AR}-OH bond, without promoting unwanted ring reactions or compromising the stability of bulk oxide, something unattainable with copper oxide catalysts (a metal with hydrogenating characteristics). Therefore, in the present study, both the use of carbon support (activated carbon) and the addition of Cu were demonstrated to influence the phenol conversion while maintaining high selectivity along the DDO pathway. The most active catalysts were deactivated during the stability test, though the product distribution was not affected, as the selectivity remained high to benzene. The used catalysts were characterized by XRD and, according to the results, it is assumed that the deactivation is linked to the blocking of active sites by carbon formation on the catalyst surface.

CRediT authorship contribution statement

Débora Dionizio: Writing - original draft, Data curation, Investigation, Formal analysis. **Leticia Forrer:** Investigation, Visualization, Formal analysis. **Gilles Berhault:** Validation, Visualization, Investigation, Supervision, Writing - review & editing. **Priscilla M. de Souza:** Conceptualization, Validation, Visualization, Investigation, Supervision, Writing - review & editing. **Cristiane A. Henriques:** Conceptualization, Validation, Visualization, Investigation, Supervision, Writing - review & editing.

Declaration of Competing Interest

The authors declare that they have no known competing financial interests or personal relationships that could have appeared to influence the work reported in this paper.

Acknowledgments

Débora G. B. Dionizio thanks CAPES (Coordenação de Aperfeiçoamento de Pessoal de Nível Superior – Brazil – PDSE Program) for financial support to her doctorate internship at IRCELYON (Institut de Recherches sur la Catalyse et l'Environnement de Lyon). Cristiane A. Henriques thanks CNPq (Conselho Nacional de Desenvolvimento Científico e Tecnológico), FAPERJ (Fundação Carlos Chagas Filho de Amparo à Pesquisa do Estado do Rio de Janeiro), and Prociência Program (Universidade do Estado do Rio de Janeiro) for the financial support. The authors also thank Nucat (Núcleo de Catálise/COPPE/UFRJ), LCPMA (Laboratório de Catálise em Petróleo e Meio Ambiente), and IRCELYON for the physicochemical analysis. This work is dedicated to the memory of Prof. Dr. Victor Teixeira da Silva that was the great mentor of this research.

References

[1] M. Asadullah, Barriers of commercial power generation using biomass gasification gas: A review, Renew. Sustain. Energy Rev. 29 (2014) 201–215. https://doi.org/10.1016/j.rser.2013.08.074.

[2] R. Shu, R. Li, B. Lin, C. Wang, Z. Cheng, Y. Chen, A review on the catalytic hydrodeoxygenation of lignin-derived phenolic compounds and the conversion of raw lignin to hydrocarbon liquid fuels, Biomass Bioenergy. 132 (2020) 105432. https://doi.org/10.1016/j.biombioe.2019.105432.

[3] Z. Usmani, M. Sharma, A.K. Awasthi, N. Sivakumar, T. Lukk, L. Pecoraro, V.K. Thakur, D. Roberts, J. Newbold, V.K. Gupta, Bioprocessing of waste biomass for sustainable product development and minimizing environmental impact, Bioresour. Technol. 322 (2021) 124548. https://doi.org/10.1016/j.biortech.2020.124548.

[4] Y.-K. Park, J.-M. Ha, S. Oh, J. Lee, Bio-oil upgrading through hydrogen transfer reactions in supercritical solvents, Chem. Eng. J. 404 (2021) 126527. https://doi.org/10.1016/j.cej.2020.126527.

[5] Z. He, X. Wang, Hydrodeoxygenation of model compounds and catalytic systems for pyrolysis bio-oils upgrading, Catal. Sustain. Energy. 1 (2012). https://doi.org/10.2478/cse-2012-0004.

[6] H. Pourzolfaghar, F. Abnisa, W.M.A. Wan Daud, M.K. Aroua, Atmospheric hydrodeoxygenation of bio-oil oxygenated model compounds: A review, J. Anal. Appl. Pyrolysis. 133 (2018) 117–127. https://doi.org/10.1016/j.jaap.2018.04.013.

[7] S. Kim, E.E. Kwon, Y.T. Kim, S. Jung, H.J. Kim, G.W. Huber, J. Lee, Recent advances in hydrodeoxygenation of biomass-derived oxygenates over heterogeneous catalysts, Green Chem. 21 (2019) 3715–3743. https://doi.org/10.1039/C9GC01210A.

[8] A.N. Kay Lup, F. Abnisa, W.M.A.W. Daud, M.K. Aroua, A review on reaction mechanisms of metal-catalyzed deoxygenation process in bio-oil model compounds, Appl. Catal. Gen. 541 (2017) 87–106. https://doi.org/10.1016/j.apcata.2017.05.002.
[9] Z. Si, X. Zhang, C. Wang, L. Ma, R. Dong, An Overview on Catalytic Hydrodeoxygenation of Pyrolysis Oil and Its Model Compounds, Catalysts. 7 (2017) 169. https://doi.org/10.3390/catal7060169.
[10] T. Prasomsri, T. Nimmanwudipong, Y. Román-Leshkov, Effective hydrodeoxygenation of biomass-derived oxygenates into unsaturated hydrocarbons by MoO3 using low H2 pressures, Energy Environ. Sci. 6 (2013) 1732. https://doi.org/10.1039/c3ee24360e.
[11] T. Prasomsri, M. Shetty, K. Murugappan, Y. Román-Leshkov, Insights into the catalytic activity and surface modification of MoO_3 during the hydrodeoxygenation of lignin-derived model compounds into aromatic hydrocarbons under low hydrogen pressures, Energy Env. Sci. 7 (2014) 2660–2669. https://doi.org/10.1039/C4EE00890A.
[12] M. Shetty, K. Murugappan, T. Prasomsri, W.H. Green, Y. Román-Leshkov, Reactivity and stability investigation of supported molybdenum oxide catalysts for the hydrodeoxygenation (HDO) of m-cresol, J. Catal. 331 (2015) 86–97. https://doi.org/10.1016/j.jcat.2015.07.034.
[13] B. Rahzani, M. Saidi, H.R. Rahimpour, B.C. Gates, M.R. Rahimpour, Experimental investigation of upgrading of lignin-derived bio-oil component anisole catalyzed by carbon nanotube-supported molybdenum, RSC Adv. 7 (2017) 10545–10556. https://doi.org/10.1039/C6RA26121C.
[14] V. Sharma, T. Getahun, M. Verma, A. Villa, N. Gupta, Carbon based catalysts for the hydrodeoxygenation of lignin and related molecules: A powerful tool for the generation of non-petroleum chemical products including hydrocarbons, Renew. Sustain. Energy Rev. 133 (2020) 110280. https://doi.org/10.1016/j.rser.2020.110280.
[15] M.M. Ambursa, J.C. Juan, Y. Yahaya, Y.H. Taufiq-Yap, Y.-C. Lin, H.V. Lee, A review on catalytic hydrodeoxygenation of lignin to transportation fuels by using nickel-based catalysts, Renew. Sustain. Energy Rev. 138 (2021) 110667. https://doi.org/10.1016/j.rser.2020.110667.
[16] A.N. Kay Lup, F. Abnisa, W.M.A. Wan Daud, M.K. Aroua, A review on reactivity and stability of heterogeneous metal catalysts for deoxygenation of bio-oil model compounds, J. Ind. Eng. Chem. 56 (2017) 1–34. https://doi.org/10.1016/j.jiec.2017.06.049.
[17] C.A. Teles, P.M. de Souza, R.C. Rabelo-Neto, A. Teran, G. Jacobs, C. Vilela Weikert, Z.M. Magriotis, V.O.O. Gonçalves, D.E. Resasco, F.B. Noronha, Reaction pathways for the HDO of guaiacol over supported Pd catalysts: Effect of support type in the deoxygenation of hydroxyl and methoxy groups, Mol. Catal. 523 (2022) 111491. https://doi.org/10.1016/j.mcat.2021.111491.
[18] X. Li, X. Luo, Y. Jin, J. Li, H. Zhang, A. Zhang, J. Xie, Heterogeneous sulfur-free hydrodeoxygenation catalysts for selectively upgrading the renewable bio-oils to second generation biofuels, Renew. Sustain. Energy Rev. 82 (2018) 3762–3797. https://doi.org/10.1016/j.rser.2017.10.091.
[19] M.C. Alvarez-Galvan, G. Blanco-Brieva, M. Capel-Sanchez, S. Morales-delaRosa, J.M. Campos-Martin, J.L.G. Fierro, Metal phosphide catalysts for the hydrotreatment of non-edible vegetable oils, Catal. Today. 302 (2018) 242–249. https://doi.org/10.1016/j.cattod.2017.03.031.
[20] Z. Cai, F. Wang, X. Zhang, R. Ahishakiye, Y. Xie, Y. Shen, Selective hydrodeoxygenation of guaiacol to phenolics over activated carbon supported molybdenum catalysts, Mol. Catal. 441 (2017) 28–34. https://doi.org/10.1016/j.mcat.2017.07.024.
[21] S. Ansaloni, N. Russo, R. Pirone, Hydrodeoxygenation of guaiacol over molybdenum-based catalysts: The effect of support and the nature of the active site, Can. J. Chem. Eng. 95 (2017) 1730–1744. https://doi.org/10.1002/cjce.22819.
[22] M. Shetty, K. Murugappan, W.H. Green, Y. Román-Leshkov, Structural Properties and Reactivity Trends of Molybdenum Oxide Catalysts Supported on Zirconia for the Hydrodeoxygenation of Anisole, ACS Sustain. Chem. Eng. 5 (2017) 5293–5301. https://doi.org/10.1021/acssuschemeng.7b00642.

[23] M. Saidi, F. Samimi, D. Karimipourfard, T. Nimmanwudipong, B.C. Gates, M.R. Rahimpour, Upgrading of lignin-derived bio-oils by catalytic hydrodeoxygenation, Energy Env. Sci. 7 (2014) 103–129. https://doi.org/10.1039/C3EE43081B.
[24] Z. Pan, R. Wang, M. Li, Y. Chu, J. Chen, Deoxygenation of methyl laurate to hydrocarbons on silica-supported Ni-Mo phosphides: Effect of calcination temperatures of precursor, J. Energy Chem. 24 (2015) 77–86. https://doi.org/10.1016/S2095-4956(15)60287-X.
[25] S. Kasiraju, L.C. Grabow, Learning from the past: Are catalyst design principles transferrable between hydrodesulfurization and deoxygenation?, AIChE J. 64 (2018) 3121–3133. https://doi.org/10.1002/aic.16151.
[26] G.G. Gonzalez, P.C. Zonetti, E.B. Silveira, F.M.T. Mendes, R.R. de Avillez, C.R.K. Rabello, F.M.Z. Zotin, L.G. Appel, Two mechanisms for acetic acid synthesis from ethanol and water, J. Catal. 380 (2019) 343–351. https://doi.org/10.1016/j.jcat.2019.09.031.
[27] T.A. Saleh, G.I. Danmaliki, Influence of acidic and basic treatments of activated carbon derived from waste rubber tires on adsorptive desulfurization of thiophenes, J. Taiwan Inst. Chem. Eng. 60 (2016) 460–468. https://doi.org/10.1016/j.jtice.2015.11.008.
[28] F.G.F. de Paula, I. Campello-Gómez, P.F.R. Ortega, F. Rodríguez-Reinoso, M. Martínez-Escandell, J. Silvestre-Albero, Structural Flexibility in Activated Carbon Materials Prepared under Harsh Activation Conditions, Materials. 12 (2019) 1988. https://doi.org/10.3390/ma12121988.
[29] Z. Zhu, Z. Liu, S. Liu, H. Niu, T. Hu, T. Liu, Y. Xie, NO reduction with NH3 over an activated carbon-supported copper oxide catalysts at low temperatures, Appl. Catal. B Environ. 26 (2000) 25–35. https://doi.org/10.1016/S0926-3373(99)00144-7.
[30] G. Zhang, Z. Li, H. Zheng, T. Fu, Y. Ju, Y. Wang, Influence of the surface oxygenated groups of activated carbon on preparation of a nano Cu/AC catalyst and heterogeneous catalysis in the oxidative carbonylation of methanol, Appl. Catal. B Environ. 179 (2015) 95–105. https://doi.org/10.1016/j.apcatb.2015.05.001.
[31] C. Thomazeau, V. Martin, P. Afanasiev, Effect of support on the thermal decomposition of (NH4)6Mo7O24·4H2O in the inert gas atmosphere, Appl. Catal. Gen. 199 (2000) 61–72. https://doi.org/10.1016/S0926-860X(99)00523-2.
[32] J. Chang, T. Danuthai, S. Dewiyanti, C. Wang, A. Borgna, Hydrodeoxygenation of Guaiacol over Carbon-Supported Metal Catalysts, ChemCatChem. 5 (2013) 3041–3049. https://doi.org/10.1002/cctc.201300096.
[33] H. Kirakosyan, K. Nazaretyan, S. Aydinyan, S. Kharatyan, The Mechanism of Joint Reduction of MoO3 and CuO by Combined Mg/C Reducer at High Heating Rates, J. Compos. Sci. 5 (2021) 318. https://doi.org/10.3390/jcs5120318.
[34] M.C. Biesinger, Advanced analysis of copper X-ray photoelectron spectra: Advanced analysis of copper X-ray photoelectron spectra, Surf. Interface Anal. 49 (2017) 1325–1334. https://doi.org/10.1002/sia.6239.
[35] K. Murugappan, E.M. Anderson, D. Teschner, T.E. Jones, K. Skorupska, Y. Román-Leshkov, Operando NAP-XPS unveils differences in MoO3 and Mo2C during hydrodeoxygenation, Nat. Catal. 1 (2018) 960–967. https://doi.org/10.1038/s41929-018-0171-9.
[36] P.A. Spevack, N.S. McIntyre, Thermal Reduction of MOO, J. Phys. Chem. 96 (1992) 9029–9035. https://doi.org/10.1021/j100201a062.
[37] J. Zhang, B. Fidalgo, D. Shen, X. Zhang, S. Gu, Mechanism of hydrodeoxygenation (HDO) in anisole decomposition over metal loaded Brønsted acid sites: Density Functional Theory (DFT) study, Mol. Catal. 454 (2018) 30–37. https://doi.org/10.1016/j.mcat.2018.05.015.
[38] G. Mestl, T.K.K. Srinivasan, Raman Spectroscopy of Monolayer-Type Catalysts: Supported Molybdenum Oxides, Catal. Rev. 40 (1998) 451–570. https://doi.org/10.1080/01614949808007114.
[39] M. Dieterle, G. Weinberg, G. Mestl, Raman spectroscopy of molybdenum oxides, Phys. Chem. Chem. Phys. 4 (2002) 812–821. https://doi.org/10.1039/b107012f.
[40] S. Wei, X. Kong, H. Wang, Y. Mao, M. Chao, J. Guo, E. Liang, Negative thermal expansion property of CuMoO4, Optik. 160 (2018) 61–67. https://doi.org/10.1016/j.ijleo.2018.01.105.
[41] Y. Deng, A.D. Handoko, Y. Du, S. Xi, B.S. Yeo, *In Situ* Raman Spectroscopy of Copper and Copper Oxide Surfaces during Electrochemical Oxygen Evolution Reaction: Identification of

Cu ^{III} Oxides as Catalytically Active Species, ACS Catal. 6 (2016) 2473–2481. https://doi.org/10.1021/acscatal.6b00205.
[42] M.S. Dresselhaus, A. Jorio, M. Hofmann, G. Dresselhaus, R. Saito, Perspectives on Carbon Nanotubes and Graphene Raman Spectroscopy, Nano Lett. 10 (2010) 751–758. https://doi.org/10.1021/nl904286r.
[43] W. Wen, L. Jing, M.G. White, N. Marinkovic, J.C. Hanson, J.A. Rodriguez, In situ time-resolved characterization of novel Cu–MoO2 catalysts during the water–gas shift reaction, Catal. Lett. 113 (2007) 1–6. https://doi.org/10.1007/s10562-006-9003-7.
[44] E.V. Soltys, Kh.Kh. Urazov, T.S. Kharlamova, O.V. Vodyankina, Redox and Catalytic Properties of Copper Molybdates with Various Composition, Kinet. Catal. 59 (2018) 58–69. https://doi.org/10.1134/S0023158418010111.
[45] J. Díez-Ramírez, P. Sánchez, A. Rodríguez-Gómez, J.L. Valverde, F. Dorado, Carbon Nanofiber-Based Palladium/Zinc Catalysts for the Hydrogenation of Carbon Dioxide to Methanol at Atmospheric Pressure, Ind. Eng. Chem. Res. 55 (2016) 3556–3567. https://doi.org/10.1021/acs.iecr.6b00170.
[46] L. Feng, X. Li, D.B. Dadyburjor, E.L. Kugler, A Temperature-Programmed-Reduction Study on Alkali-Promoted, Carbon-Supported Molybdenum Catalysts, J. Catal. 190 (2000) 1–13. https://doi.org/10.1006/jcat.1999.2744.
[47] J. Zhu, F. Gao, L. Dong, W. Yu, L. Qi, Z. Wang, L. Dong, Y. Chen, Studies on surface structure of MxOy/MoO3/CeO2 system (M=Ni, Cu, Fe) and its influence on SCR of NO by NH3, Appl. Catal. B Environ. 95 (2010) 144–152. https://doi.org/10.1016/j.apcatb.2009.12.021.
[48] B. Chen, Y. Ma, L. Ding, L. Xu, Z. Wu, Q. Yuan, W. Huang, Reactivity of Hydroxyls and Water on a CeO_2 (111) Thin Film Surface: The Role of Oxygen Vacancy, J. Phys. Chem. C. 117 (2013) 5800–5810. https://doi.org/10.1021/jp312406f.
[49] B. Voss, N.C. Schjødt, J.-D. Grunwaldt, S.I. Andersen, J.M. Woodley, Kinetics of acetic acid synthesis from ethanol over a Cu/SiO2 catalyst, Appl. Catal. Gen. 402 (2011) 69–79. https://doi.org/10.1016/j.apcata.2011.05.030.
[50] C. Tsai, K. Lee, J.S. Yoo, X. Liu, H. Aljama, L.D. Chen, C.F. Dickens, T.S. Geisler, C.J. Guido, T.M. Joseph, C.S. Kirk, A.A. Latimer, B. Loong, R.J. McCarty, J.H. Montoya, L. Power, A.R. Singh, J.J. Willis, M.M. Winterkorn, M. Yuan, Z.-J. Zhao, J. Wilcox, J.K. Nørskov, Direct Water Decomposition on Transition Metal Surfaces: Structural Dependence and Catalytic Screening, Catal. Lett. 146 (2016) 718–724. https://doi.org/10.1007/s10562-016-1708-7.
[51] A.A. Phatak, W.N. Delgass, F.H. Ribeiro, W.F. Schneider, Density Functional Theory Comparison of Water Dissociation Steps on Cu, Au, Ni, Pd, and Pt, J. Phys. Chem. C. 113 (2009) 7269–7276. https://doi.org/10.1021/jp810216b.
[52] M.T. Greiner, L. Chai, M.G. Helander, W.-M. Tang, Z.-H. Lu, Metal/Metal-Oxide Interfaces: How Metal Contacts Affect the Work Function and Band Structure of MoO_3, Adv. Funct. Mater. 23 (2013) 215–226. https://doi.org/10.1002/adfm.201200993.
[53] V. Korpelin, M.M. Melander, K. Honkala, Reducing the Irreducible: Dispersed Metal Atoms Facilitate Reduction of Irreducible Oxides, J. Phys. Chem. C. 126 (2022) 933–945. https://doi.org/10.1021/acs.jpcc.1c08979.
[54] A. Ruiz Puigdollers, P. Schlexer, S. Tosoni, G. Pacchioni, Increasing Oxide Reducibility: The Role of Metal/Oxide Interfaces in the Formation of Oxygen Vacancies, ACS Catal. 7 (2017) 6493–6513. https://doi.org/10.1021/acscatal.7b01913.
[55] Y. Li, Y. Zhang, K. Qian, W. Huang, Metal–Support Interactions in Metal/Oxide Catalysts and Oxide–Metal Interactions in Oxide/Metal Inverse Catalysts, ACS Catal. 12 (2022) 1268–1287. https://doi.org/10.1021/acscatal.1c04854.
[56] V.M.L. Whiffen, K.J. Smith, Hydrodeoxygenation of 4-Methylphenol over Unsupported MoP, MoS_2, and MoO_x Catalysts, Energy Fuels. 24 (2010) 4728–4737. https://doi.org/10.1021/ef901270h.
[57] D. Raikwar, M. Munagala, S. Majumdar, D. Shee, Hydrodeoxygenation of guaiacol over Mo, W and Ta modified supported nickel catalysts, Catal. Today. 325 (2019) 117–130. https://doi.org/10.1016/j.cattod.2018.09.039.
[58] V.O.O. Gonçalves, C. Ciotonea, S. Arrii-Clacens, N. Guignard, C. Roudaut, J. Rousseau, J.-M. Clacens, S. Royer, F. Richard, Effect of the support on the hydrodeoxygenation of m -cresol

over molybdenum oxide based catalysts, Appl. Catal. B Environ. 214 (2017) 57–66. https://doi.org/10.1016/j.apcatb.2017.05.003.
[59] C. Ranga, R. Lødeng, V.I. Alexiadis, T. Rajkhowa, H. Bjørkan, S. Chytil, I.H. Svenum, J. Walmsley, C. Detavernier, H. Poelman, P. Van Der Voort, J.W. Thybaut, Effect of composition and preparation of supported MoO3 catalysts for anisole hydrodeoxygenation, Chem. Eng. J. 335 (2018) 120–132. https://doi.org/10.1016/j.cej.2017.10.090.
[60] R. Lødeng, C. Ranga, T. Rajkhowa, V.I. Alexiadis, H. Bjørkan, S. Chytil, I.H. Svenum, J. Walmsley, J.W. Thybaut, Hydrodeoxygenation of phenolics in liquid phase over supported MoO3 and carburized analogues, Biomass Convers. Biorefinery. 7 (2017) 343–359. https://doi.org/10.1007/s13399-017-0252-z.
[61] X. Zhang, J. Tang, Q. Zhang, Q. Liu, Y. Li, L. Chen, C. Wang, L. Ma, Hydrodeoxygenation of lignin-derived phenolic compounds into aromatic hydrocarbons under low hydrogen pressure using molybdenum oxide as catalyst, Catal. Today. 319 (2019) 41–47. https://doi.org/10.1016/j.cattod.2018.03.068.
[62] X. Zhang, Q. Liu, Q. Zhang, Q. Liu, L. Chen, Y. Li, C. Wang, L. Ma, Aromatic fuel production from phenolics by catalytic hydrodeoxygenation over novel Mo-based catalyst, Energy Procedia. 158 (2019) 984–990. https://doi.org/10.1016/j.egypro.2019.01.240.
[63] M. Shetty, E.M. Anderson, W.H. Green, Y. Román-Leshkov, Kinetic analysis and reaction mechanism for anisole conversion over zirconia-supported molybdenum oxide, J. Catal. 376 (2019) 248–257. https://doi.org/10.1016/j.jcat.2019.06.046.
[64] R. Ding, Y. Wu, Y. Chen, J. Liang, J. Liu, M. Yang, Effective hydrodeoxygenation of palmitic acid to diesel-like hydrocarbons over MoO 2 /CNTs catalyst, Chem. Eng. Sci. 135 (2015) 517–525. https://doi.org/10.1016/j.ces.2014.10.024.
[65] L.-B. Sun, Z.-M. Zong, J.-H. Kou, G.-F. Liu, X. Sun, X.-Y. Wei, G.-J. Zhou, C.W. Lee, Activated Carbon-Catalyzed Hydrogen Transfer to α,ω-Diarylalkanes, Energy Fuels. 19 (2005) 1–6. https://doi.org/10.1021/ef0497964.
[66] Y. Wang, Y. Wang, Q. Tang, F. Jing, Q. Cao, W. Fang, Efficient activation of H2 on copper species immobilized by MCM-41 for selective hydrogenation of furfural at ambient pressure, Mol. Catal. 515 (2021) 111921. https://doi.org/10.1016/j.mcat.2021.111921.
[67] J. Lee, J.H. Seo, C. Nguyen-Huy, E. Yang, J.G. Lee, H. Lee, E.J. Jang, J.H. Kwak, J.H. Lee, H. Lee, K. An, Cu2O(100) surface as an active site for catalytic furfural hydrogenation, Appl. Catal. B Environ. 282 (2021) 119576. https://doi.org/10.1016/j.apcatb.2020.119576.
[68] G.-H. Liu, Z.-M. Zong, Z.-Q. Liu, F.-J. Liu, Y.-Y. Zhang, X.-Y. Wei, Solvent-controlled selective hydrodeoxygenation of bio-derived guaiacol to arenes or phenols over a biochar supported Co-doped MoO2 catalyst, Fuel Process. Technol. 179 (2018) 114–123. https://doi.org/10.1016/j.fuproc.2018.05.035.
[69] V. Itthibenchapong, P. Chakthranont, C. Sattayanon, T. Butburee, K. Faungnawakij, S. Namuangruk, Understanding the promoter effect of bifunctional (Pt, Ni, Cu)-MoO3-x/TiO2 catalysts for the hydrodeoxygenation of p-cresol: A combined DFT and experimental study, Appl. Surf. Sci. 547 (2021) 149170. https://doi.org/10.1016/j.apsusc.2021.149170.
[70] A. Bjelić, M. Grilc, M. Huš, B. Likozar, Hydrogenation and hydrodeoxygenation of aromatic lignin monomers over Cu/C, Ni/C, Pd/C, Pt/C, Rh/C and Ru/C catalysts: Mechanisms, reaction micro-kinetic modelling and quantitative structure-activity relationships, Chem. Eng. J. 359 (2019) 305–320. https://doi.org/10.1016/j.cej.2018.11.107.
[71] R. Shu, B. Lin, J. Zhang, C. Wang, Z. Yang, Y. Chen, Efficient catalytic hydrodeoxygenation of phenolic compounds and bio-oil over highly dispersed Ru/TiO2, Fuel Process. Technol. 184 (2019) 12–18. https://doi.org/10.1016/j.fuproc.2018.11.004.
[72] C.A. Teles, R.C. Rabelo-Neto, G. Jacobs, B.H. Davis, D.E. Resasco, F.B. Noronha, Hydrodeoxygenation of Phenol over Zirconia-Supported Catalysts: The Effect of Metal Type on Reaction Mechanism and Catalyst Deactivation, ChemCatChem. 9 (2017) 2850–2863. https://doi.org/10.1002/cctc.201700047.
[73] A.B. Dongil, B. Bachiller-Baeza, I. Rodríguez-Ramos, J.L.G. Fierro, N. Escalona, The effect of Cu loading on Ni/carbon nanotubes catalysts for hydrodeoxygenation of guaiacol, RSC Adv. 6 (2016) 26658–26667. https://doi.org/10.1039/C6RA00041J.

[74] P.M. de Souza, R.C. Rabelo-Neto, L.E.P. Borges, G. Jacobs, B.H. Davis, D.E. Resasco, F.B. Noronha, Hydrodeoxygenation of Phenol over Pd Catalysts. Effect of Support on Reaction Mechanism and Catalyst Deactivation, ACS Catal. 7 (2017) 2058–2073. https://doi.org/10.1021/acscatal.6b02022.
[75] A.M. Barrios, C.A. Teles, P.M. de Souza, R.C. Rabelo-Neto, G. Jacobs, B.H. Davis, L.E.P. Borges, F.B. Noronha, Hydrodeoxygenation of phenol over niobia supported Pd catalyst, Catal. Today. 302 (2018) 115–124. https://doi.org/10.1016/j.cattod.2017.03.034.
[76] L. Nie, D.E. Resasco, Kinetics and mechanism of m-cresol hydrodeoxygenation on a Pt/SiO2 catalyst, J. Catal. 317 (2014) 22–29. https://doi.org/10.1016/j.jcat.2014.05.024.
[77] P.M. Mortensen, J.-D. Grunwaldt, P.A. Jensen, A.D. Jensen, Screening of Catalysts for Hydrodeoxygenation of Phenol as a Model Compound for Bio-oil, ACS Catal. 3 (2013) 1774–1785. https://doi.org/10.1021/cs400266e.
[78] P.-J. Hsu, J.-W. Jiang, Y.-C. Lin, Does a Strong Oxophilic Promoter Enhance Direct Deoxygenation? A Study of NiFe, NiMo, and NiW Catalysts in *p* -Cresol Conversion, ACS Sustain. Chem. Eng. 6 (2018) 660–667. https://doi.org/10.1021/acssuschemeng.7b03010.
[79] Q. Hu, L. Yang, G. Fan, F. Li, Hydrogenation of biomass-derived compounds containing a carbonyl group over a copper-based nanocatalyst: Insight into the origin and influence of surface oxygen vacancies, J. Catal. 340 (2016) 184–195. https://doi.org/10.1016/j.jcat.2016.05.008.
[80] S. Kim, Y.F. Tsang, E.E. Kwon, K.-Y.A. Lin, J. Lee, Recently developed methods to enhance stability of heterogeneous catalysts for conversion of biomass-derived feedstocks, Korean J. Chem. Eng. 36 (2019) 1–11. https://doi.org/10.1007/s11814-018-0174-x.
[81] P.M. de Souza, C.V.M. Inocêncio, V.I. Perez, R.C. Rabelo-Neto, V.O.O. Gonçalves, G. Jacobs, F. Richard, V.T. da Silva, F.B. Noronha, Hydrodeoxygenation of phenol using nickel phosphide catalysts. Study of the effect of the support, Catal. Today. 356 (2020) 366–375. https://doi.org/10.1016/j.cattod.2019.08.028.
[82] P. Yan, M. Drewery, J. Mensah, J.C. Mackie, E. Kennedy, M. Stockenhuber, Study on Catalyst Deactivation During the Hydrodeoxygenation of Model Compounds, Top. Catal. 63 (2020) 778–792. https://doi.org/10.1007/s11244-020-01310-2.
[83] D. Gao, C. Schweitzer, H.T. Hwang, A. Varma, Conversion of Guaiacol on Noble Metal Catalysts: Reaction Performance and Deactivation Studies, Ind. Eng. Chem. Res. 53 (2014) 18658–18667. https://doi.org/10.1021/ie500495z.
[84] M.Á. González-Borja, D.E. Resasco, Anisole and Guaiacol Hydrodeoxygenation over Monolithic Pt–Sn Catalysts, Energy Fuels. 25 (2011) 4155–4162. https://doi.org/10.1021/ef200728r.
[85] C. Yu, S. Yu, L. Li, S. Li, Highly stable Mo-based catalysts for selective hydrodeoxygenation to produce diesel-like hydrocarbons, Fuel. 323 (2022) 124334. https://doi.org/10.1016/j.fuel.2022.124334.